A review of cloud top height and optical depth histograms from MISR, ISCCP, and MODIS

Roger Marchand,[1] Thomas Ackerman,[1] Mike Smyth,[2] and William B. Rossow[3]

Received 21 October 2009; revised 23 March 2010; accepted 12 April 2010; published 24 August 2010.

[1] There are notable differences in the joint histograms of cloud top height and optical depth being produced from the Moderate Resolution Imaging Spectroradiometer (MODIS) and the Multiangle Imaging Spectro-Radiometer (MISR) and by the International Satellite Cloud Climatology Project (ISCCP). These differences have their roots in the different retrieval approaches used by the three projects and are driven largely by responses of the retrievals to (1) stratocumulus (or more broadly low-level clouds under temperature inversions), (2) small (subpixel) or broken low-level clouds, and (3) multilayer clouds. Because each data set has different strengths and weakness, the combination tells us more about the observed cloud fields than any of the three by itself. In particular, the MISR stereo height retrieval provides a calibration insensitive approach to determining cloud height that is especially valuable in combination with ISCCP or MODIS because the combination provides a means to estimate the amount of multilayer cloud, where the upper cloud is optically thin. In this article we present a review of the three data sets using case studies and comparisons of annually averaged joint histograms on global and regional scales. Recommendations for using these data in climate model evaluations are provided.

Citation: Marchand, R., T. Ackerman, M. Smyth, and W. B. Rossow (2010), A review of cloud top height and optical depth histograms from MISR, ISCCP, and MODIS, *J. Geophys. Res.*, *115*, D16206, doi:10.1029/2009JD013422.

1. Introduction

[2] Joint histograms of cloud top height (CTH) and optical depth (OD) derived by the International Satellite Cloud Climatology Project (ISCCP) are being widely used by the climate modeling community in evaluating global climate models [e.g., *Webb et al.*, 2001; *Norris and Weaver*, 2001; *Lin and Zhang*, 2004; *Zhang et al.*, 2005; *Wyant et al.*, 2006]. Similar joint histograms of cloud top height and optical depth are now being produced by the NASA Multiangle Imaging Spectroradiometer (MISR) and Moderate Resolution Imaging Spectroradiometer (MODIS) instrument teams. In this article we compare these CTH-OD joint histograms on global and regional scales. While there are some broad similarities among the data sets, there are also large differences, which on the surface would seem to undermine the utility of these data for model evaluation. However, because the different data sets have different strengths and weaknesses, we find that the combination tells us more about the observed clouds than any one data set by itself.

[3] The differences have their roots in the different algorithms used both to detect clouds and to retrieve the cloud height and optical depth. In this article, we provide a review the retrieval algorithms used by the three projects. Much of the difference in the retrievals can be understood from the response of the algorithms to stratocumulus, trade cumulus and multilayer clouds. Thus after describing the algorithms in section 2, in section 3 we examine the retrieval results for typical stratocumulus, trade cumulus and multilayer cloud scenes. Using these examples as a guide, in section 4 we then compare the ISCCP, MISR and MODIS data sets globally with specific focus on the North Pacific and the tropical western Pacific.

[4] The MISR retrieval is only run over ocean surfaces and so our analysis is restricted to oceanic regions. The comparison highlights the strengths and weaknesses of each data set and examples are given showing how the data sets can be combined to yield additional information on the frequency of multilayer clouds. Specific recommendations on how these data should be used for the analysis of global climate model output are provided in section 5. These recommendations are used in an examination of the Multiscale Modeling Framework (MMF) climate model in a companion paper to this article [*Marchand and Ackerman*, 2010].

[5] The ISCCP and MODIS projects report the position of cloud top in pressure coordinates while the MISR project reports the altitude of cloud top in distance above the surface (i.e., meters). In many of the comparisons in this article we convert the MISR cloud top altitude to an equivalent cloud top pressure. We use the expression cloud top pressure (CTP) when referring explicitly to cloud top in pressure

[1] Joint Institute for the Study of the Atmosphere and Ocean, University of Washington, Seattle, Washington, USA.
[2] Jet Propulsion Laboratory, Pasadena, California, USA.
[3] NOAA Cooperative Remote Sensing Science and Technology Center, City College of New York, New York, New York, USA.

0148-0227/10/2009JD013422

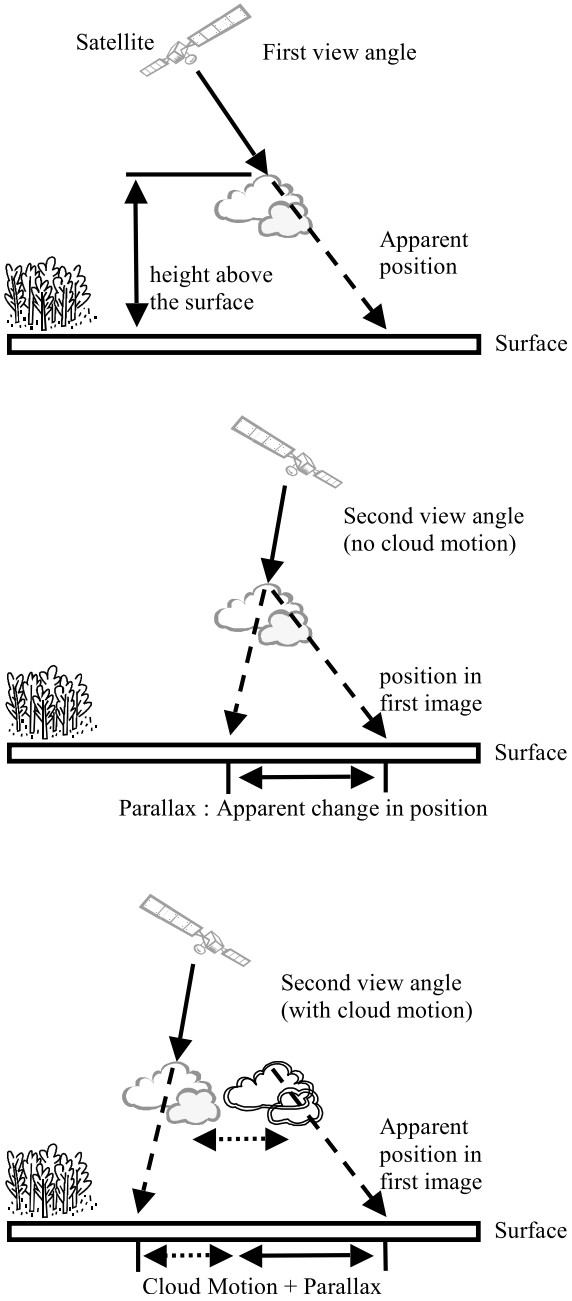

Figure 1. Depiction of cloud parallax with and without cloud motion/clouds winds [from *Marchand et al.*, 2007].

coordinates, and use the expression cloud top height (CTH) in a more general sense to mean either cloud top pressure or cloud top altitude.

2. Description of ISCCP, MISR, and MODIS Retrievals

2.1. International Satellite Cloud Climatology Project

[6] Since July of 1983, ISCCP has been collecting data from a suite of weather satellites (both geostationary and polar orbiting) and has used these data to generate joint histograms of cloud top pressure (CTP) and cloud optical depth (OD) [*Rossow and Schiffer*, 1999]. ISCCP uses the observed infrared (IR) brightness temperature to determine cloud top temperature, from which cloud top pressure is inferred using an atmospheric profile that relates temperature to pressure. This approach initially assumes the cloud top is opaque (radiates like a blackbody) and entirely covers the satellite pixel over which the retrieval is applied. If, however, the cloud is found to have a low optical depth, the cloud top height is later adjusted based on the retrieved optical depth. The optical depth is determined from a single narrow-band visible channel near 0.6 μm, except over snow and ice where 3.75 μm observations are also used. The retrieval assumes a single-layer cloud composed of either 10 μm (effective radius) water droplets (when the cloud top IR temperature is 260 K or greater) or 30 μm (effective radius) ice crystals (with an aggregate-like shape). The conversion of observed radiance to optical depth is based on one-dimensional radiative transfer and aerosols are not considered. The contribution of the surface to the observed visible radiance is modeled using observations gathered at other times, which are identified as clear-sky, in combination with an anisotropic model over the oceans and an isotropic surface assumption over land areas. The clear or cloud identification is based on a combination of visible reflectance and infrared brightness thresholds determined from a statistical analysis of observations gathered over an extended period.

2.2. Multiangle Imaging Spectroradiometer

[7] MISR is one of five instruments (including MODIS) on board the NASA Terra satellite, which was launched in December of 1999 [*Diner et al.*, 2002, 2005]. The Terra satellite is in a Sun-synchronous orbit with an equatorial crossing time of about 10:30 A.M. The MISR instrument consists of nine cameras, each of which makes images with approximately 275 m sampling in four narrow spectral bands located at 443, 555, 670, and 865 nm. These cameras collect data at nine view angles (nadir plus 26.1, 45.6, 60.0, and 70.5 degrees forward and aft of the direction of flight).

[8] MISR determines cloud top height (CTH) using a stereo-imaging technique, as depicted in Figure 1 [*Moroney et al.*, 2002; *Muller et al.*, 2002]. A significant advantage of the MISR CTH retrieval is that the technique is geometric and is not sensitive to the actual value of the observed radiances (i.e., the sensor calibration). The MISR CTH retrieval has been the focus of several studies including those by *Marchand et al.* [2007], *Naud et al.* [2002, 2004, 2005], *Seiz et al.* [2006], and *Marchand et al.* [2001]. These studies show that when a cloud is detected, the cloud top is found with little bias and a standard deviation of about 1000 m. The dominant source of error in the height retrieval comes from errors in the wind correction (or lack thereof). We will discuss the impact of this uncertainty on the joint histograms further in the next section. The MISR retrieval for optical depth is similar to that of ISCCP in that the optical depth is retrieved from the observed visible radiance assuming a one-dimensional single-layer cloud with a fixed effective radius and no aerosols. The MISR OD retrieval differs from ISCCP in that it is only run over ocean surfaces and is based on observations at 865 nm, which has relatively

little surface reflectance over the deep oceans. The optical depth retrieval is only run for pixels determined to be cloudy (with high confidence) by the MISR radiometric cloud mask, described by *Zhao and Di Girolamo* [2004], and is restricted to ice-free oceans. Additional details on the MISR CTH-OD data set, including a brief examination of view angle dependence, are given in Appendix A.

2.3. Moderate Resolution Imaging Spectroradiometer

[9] MODIS is a 36-channel scanning radiometer with the channels (or bands) distributed between 0.415 and 14.235 μm [*King et al.*, 2003]. A MODIS instrument is on board both the NASA Terra and Aqua platforms. In this evaluation, we use only data from MODIS Terra. In the operational MODIS cloud retrieval (product name MOD06 for MODIS Terra), the optical depth and effective radius are determined simultaneously at 1 km [*Platnick et al.*, 2003]. This is accomplished using a combination of measurements in two bands. One band is in the shortwave infrared (1.6, 2.1, or 3.7 μm) where condensed cloud water has some absorption, while in the second band water is practically nonabsorbing (0.65, 0.86, or 1.2 μm). The nonabsorbing band primarily constrains the optical depth while the shortwave infrared band adds particle size information. The nonabsorbing band is chosen to minimize the underlying surface reflectance with 0.65, 0.86, and 1.2 μm chosen for land, ocean and ice/snow surfaces, respectively. The MODIS cloud top pressure retrieval is based on a combination of techniques. A CO_2 slicing technique is used to determine cloud top pressure for clouds above about 700 hPa while the cloud top pressure for low clouds is determined in a similar way to ISCCP, using the MODIS 11 μm band IR temperature in conjunction with NCEP Global Data Assimilation System (GDAS) temperature profiles [*Menzel et al.*, 2008].

[10] While the operational MODIS cloud mask (MOD35) is used by MOD06, not every pixel identified as cloudy in the 1 km MOD35 cloud mask is processed to obtain an optical depth and effective radius. In MODIS Collection 5, retrievals are attempted only for 1km pixels that (1) do not constitute the edge of a cloud as detected by the MOD35 cloud mask, (2) when over ocean, have a minimum of 50% of the 250 m pixels flagged as cloudy in the MODIS 250 m cloud mask, and (3) pass a variety of spectral tests for removal of questionable heavy aerosol or glint scenes. Because of this additional screening (referred to as "clear sky restoral" in MODIS documentation) the fraction of MOD06 pixels with a retrieved optical depth will be less than the cloud fraction that one would determine from the MOD35 cloud mask. As we will see later, the reduction is significant. Fundamentally, this reduction in coverage represents a choice on the part of the MODIS team to include only high-quality cloud property retrievals in their global summaries and the strength of the MODIS data set lies in its ability to provide estimates for cloud effective radius and other parameters that are not available or can't be as accurately determined by other satellite imagers.

[11] The MODIS CTH-OD histograms examined in section 4 are taken from the MOD08 (Level 3) monthly 1° gridded global summary product. In this article, we examine only the MOD08 ISCCP-like histograms of cloud top pressure and optical depth. The MOD08 product contains a variety of data summaries including joint histograms with effective radius. Additional details regarding MOD06 and MOD08 data sets are given in Appendix B.

3. Case Studies

[12] Before comparing cloud top height and optical depth histograms directly, we first examine the ISCCP, MODIS, and MISR retrievals that go into these histograms for several commonly occurring cloud types in order to provide some insight into the algorithms. While only a few examples are shown, we have observed characteristically similar results from many scenes drawn from orbits that passed over the Pacific and Atlantic oceans and (as will be discussed) these differences are expected outcomes the retrieval algorithms.

[13] All of the data shown in this section are taken from the ISCCP DX, MODIS MOD06 (collection 5) and MISR TC-STEREO (version F08) pixel-level products. Since MISR and MODIS sensors both fly on the Terra platform, comparisons between the two data sets are straightforward, as they observe the cloud scene at essentially the same time. The ISCCP DX data are taken from the GMS or GOES satellites gathered within 10 to 40 min of the Terra overpass. The ISCCP pixel-level DX data set is a spatially sampled version of the ISCCP data binned in the ISCCP D1 and D2 global summary data sets. The ISCCP retrieval is run at about 4 km resolution (at nadir; much lower as one approaches the edge of the sensor swath) and sampled roughly every 30 km to form the DX data set. In order to display images of the ISCCP data, we have mapped the ISCCP DX data onto the MODIS grid using a nearest neighbor approach. This is only for display purposes.

[14] In the remainder of this section, we examine three commonly occurring situations: (1) stratocumulus, (2) trade cumulus (broken boundary layer cloud), and (3) multilayer cloud featuring an optically thin upper-level cloud.

3.1. Stratocumulus

[15] Figure 2a shows an example of a stratocumulus cloud deck observed on April 25, 2001, (MISR orbit #7200, MODIS overpass 1900 UTC) off the coast of California, along with the associated ISCCP, MODIS and MISR retrieved cloud top pressures shown in Figures 2b, 2c, and 2d. MISR retrieves the distance above the surface in meters and in Figure 2d this has been converted into approximate pressure using NCEP reanalysis. Figure 2d shows that MISR retrieves a notably lower cloud height (larger cloud pressure) for this cloud deck than either ISCCP (Figure 2b) or MODIS (Figure 2c). For low clouds both ISCCP and MODIS use the IR brightness temperature to determine cloud top temperature, from which cloud top pressure is inferred using an atmospheric profile that relates temperature to pressure. However, stratocumulus clouds often exist under temperature inversions (which are sometimes quite large). The atmospheric profiles used to convert temperature to height frequently do not capture the strength or position of the inversion well, with the result that the estimated cloud top pressure is frequently biased low for these clouds. The sensitivity of IR techniques (from both imagers and sounders) to uncertainty in temperature profiles has long been recognized [e.g., *Wielicki and Coakley*, 1981; *Stubenrauch et al.*, 1999; *Wang et al.*, 1999; *Menzel et al.*, 2008; *Garay et al.*, 2008; *Holz et al.*, 2008; *Harshvardhan*

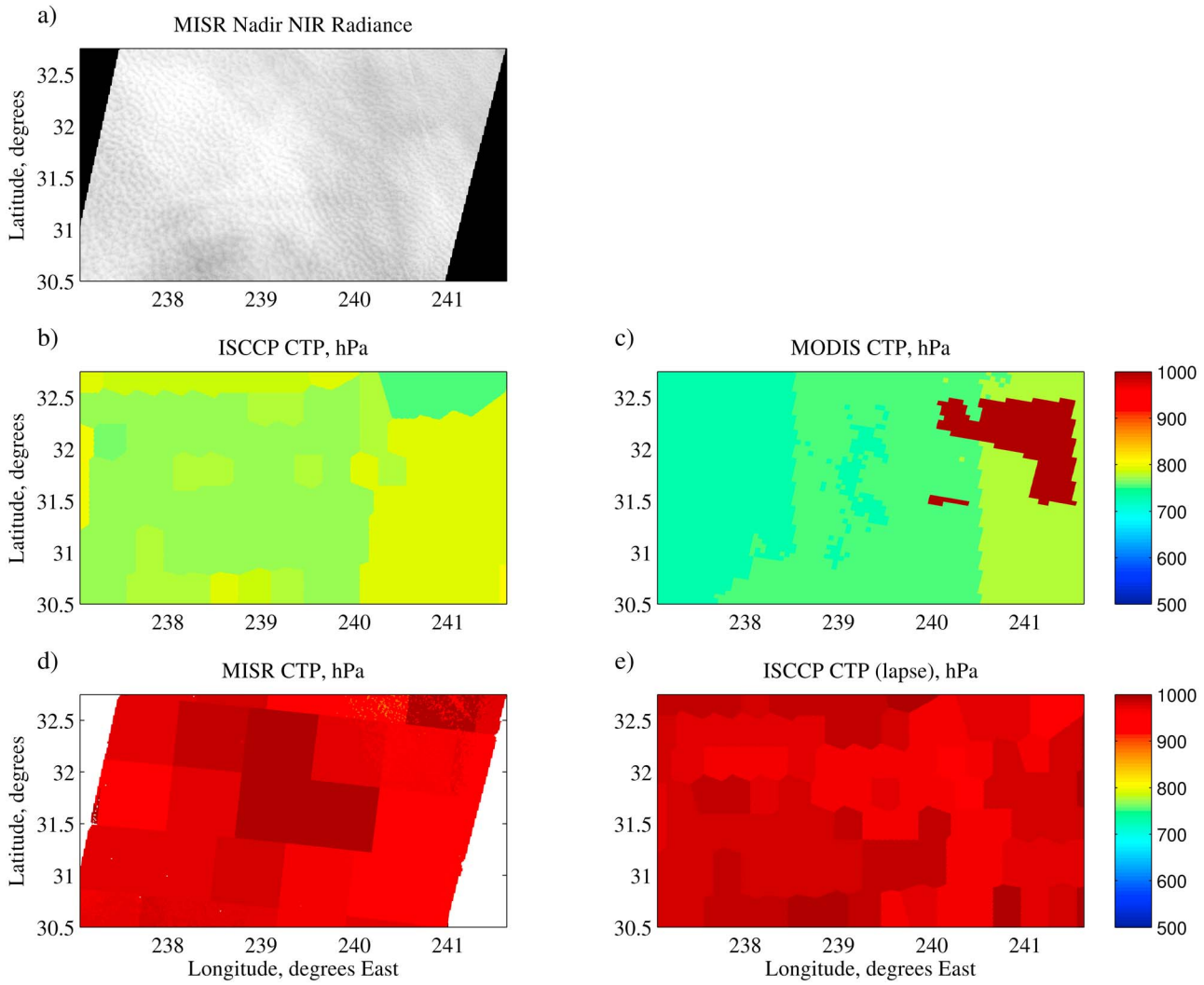

Figure 2. Cloud top pressure (CTP) retrieved by ISCCP, MODIS, and MISR for a California stratocumulus cloud observed on 25 April 2001 (MISR orbit number 7200). (a) MISR nadir view of cloud field at 865 nm, (b) ISCCP retrieved CTP, (c) MODIS (collection 5) retrieved CTP, (d) MISR retrieved height (converted into approximate pressure using NCEP reanalysis), and (e) ISCCP retrieved CTP using the lapse rate technique.

et al., 2009]. *Wang et al.* [1999] examined low clouds (primarily stratocumulus) during the ASTEX experiment and found a systematic 50–70 hPa low bias in the ISCCP cloud top pressures, while *Menzel et al.* [2008] (examining other data) noted errors in cloud top pressure up to 200 hPa. This larger error is consistent with what we observe in this example. The mean MISR cloud top pressure for the scene shown in Figure 2a is 971 hPa, while ISCCP retrieves a mean cloud top pressure of 776 hPa and MODIS 773 hPa. Averaged for all overpasses in June, July, and August, we find an average difference of about 175 hPa (roughly equivalent to 1.5 km in altitude) between MISR and ISCCP at this location. Even at the coarse vertical resolution used in the ISCCP (and MODIS) CTP-OD histograms, this bias is significant, causing cloud top to place one and sometimes two bins too high in altitude. In recently published comparisons of MODIS retrievals with active sensors, *Holz et al.* [2008] found that MODIS systematically overestimated CTH by more than 1 km for marine stratus when compared with spaceborne lidar observations from CALIPSO, while *Garay et al.* [2008] documented a 1.4 to 2 km bias in ISCCP and MODIS cloud top heights for stratocumulus off the west coast of South America, using ship-borne millimeter-wavelength cloud radar. Garay et al. also found essentially no correlation in the change of cloud top height from overpass to overpass between the radar and IR retrieved cloud tops. MISR observations for the area were found to be quite good with essentially no bias for the MISR wind-corrected heights and a bias of less than 300 m for the MISR heights without wind correction. The MISR results also showed good correlation (0.7 to 0.8) with changes in cloud top height from overpass to overpass.

[16] Comparison of MISR cloud top heights for low clouds with ground-based millimeter-wavelength cloud radar at U.S. Department of Energy Atmospheric Radiation Measurement sites in the U.S. Southern Great Plains, Barrow

Alaska, and Nauru Island in the tropical western Pacific have likewise shown good performance for both stratiform and broken clouds [*Marchand et al.*, 2007]. The MISR retrieval does, however, have a couple of limitations that affect its overall performance about which the user should be cognizant. Perhaps most significant is that (in the MISR operational code) the wind correction is assumed to be constant on domains of 70.4 km^2 and the retrieval of wind speed is sometimes noisy (primarily due to difficulties in running the pattern matching algorithms with oblique view angles). This causes the blocky or mottled appearance of the MISR retrieval in Figure 2d. In a comparison with radar-wind-profiler observations, *Hinkelman et al.* [2009] found the MISR wind retrievals have little bias but a root mean square error of about 2.5 m/s in the east-west direction and 4.5 m/s in the north-south direction compared with radar wind profiler data collected over the central United States. Only the component of the cloud velocity along the satellite ground track affects the height retrieval (which is close to north-south except at high latitudes). For the MISR operational code, each 1 m/s error in the along-track wind retrieval produces an error of about a 100 m in the cloud top height. In regard to the MISR joint histograms of cloud top height and optical depth, this means that some fraction of the counts in each cloud top height bin will be placed one bin too low or too high. In principal, this could approach 50% if the actual cloud tops in a given region predominantly occur close to one of the bin boundaries but typically should be less than about 30%. Also, because the wind retrieval is not always successful, the MISR histograms are constructed using the MISR height retrieval without wind correction when necessary, so there is likely to be a small bias in cloud top heights in locations with a predominant wind direction in the along-track direction.

[17] An alternative method for determining the cloud top pressure for ISCCP (or MODIS) is to assume a fixed temperature lapse rate (change in temperature with height) rather than relying on reanalysis (or IR soundings) to relate temperature to pressure [see *Minnis et al.*, 1992]. We note that while the ISCCP code given to users to read the D2 cloud product (the "D2READ" program) provides a utility to calculate the cloud top pressure from the cloud top and surface temperatures (using a constant lapse rate of 6.5°K/km) this program only converts the one-dimensional cloud top temperature distribution to a cloud top pressure distribution and does not correct the low clouds in the joint histograms of cloud top pressure and optical depth stored in the either the ISCCP D1 or D2 data sets. Figure 2e shows that the ISCCP cloud top pressure based on the lapse-rate technique produces a cloud top pressure (CTP) in much closer agreement to the MISR results. The mean CTP for the ISCCP lapse rate approach is 976 hPA, in good agreement with the average MISR value of 971 hPA. *Wang et al.* [1999] also noted a significant improvement using the lapse rate approach. However, these authors noted that much of the improvement in the cases they examined was due to compensating errors in the surface to cloud top temperature difference (wrong by ~2.5° K) and the actual lapse rate (observed to be ~8.3°/km). *Garay et al.* [2008] also found that the lapse rate technique represented a large improvement on average, but noted that observed lapse rate varied significantly from one Terra overpass to the next and ranged from 6.1 to 9.4°/km. Thus while one may be able to remove the bias by applying a fixed lapse rate, the spread (or distribution) of retrieved cloud top pressures may not be correctly captured using this approach. It is also likely that different locations will require different lapse rates in order to generate unbiased results.

3.2. Trade Cumulus/Broken Clouds

[18] In areas dominated by broken boundary layer clouds, we find that differences in the joint histograms of cloud top height and optical depth are largely driven by which pixels are determined to be cloudy by the detection algorithm, which of these have been deemed suitable for retrieval, and which have given rise to successful retrievals. Figure 3 shows retrieval results for a scene dominated by trade cumulus (Figure 3a), which was located to the southwest of the stratocumulus scene just examined along the same orbit (MODIS overpass 1910 UTC). Figures 3b, 3c, and 3d show the associated ISCCP, MODIS and MISR cloud top height retrievals, while Figure 3e shows the difference between the MODIS and MISR cloud top heights (for those areas where both are retrieved). Pixels without a retrieval are shown in white (which can occur because the pixel was determined to be clear or otherwise unsuitable for retrieval or because the retrieval failed).

[19] The associated joint histograms of cloud top height and optical depth for this scene are shown in Figure 4. All of these histograms are constructed from the pixel-level retrievals using only the area commonly viewed by all three sensors (i.e., only the area viewed by MISR). Figures 4a and 4b show the ISCCP and MODIS histograms, respectively, while Figures 4c and 4d show histograms constructed from MISR retrievals. In Figure 4c the MISR data are displayed using 16 vertical altitude bins (the format used in the operational MISR code), while Figure 4d shows the same result mapped onto the ISCCP and MODIS format to simplify comparison with these other data sets. The label "NR" stands for no retrieval and accounts for pixels for which there is a height retrieval but no optical depth retrieval or vice versa. At the top of each plot in Figure 4 is listed the total Cloud Fraction (CF), or more precisely, the fraction of pixels with a cloud retrieval relative to the total number of pixels. For MISR and MODIS, the fraction of pixels with either an optical depth or a cloud top height retrieval is given, followed by the fraction of pixels where both retrievals are present. For ISCCP there is always an optical depth retrieval when there is a cloud top-height retrieval. For this scene, ISCCP yields an apparent cloud fraction of 17.5%, MISR 70.5% (with 64.1% having both CTH and OD retrievals) and MODIS 55% (with only 5.8% having CTH and OD retrievals).

[20] Both *Rossow et al.* [1993] and *Rossow and Schiffer* [1999] indicate that detection errors appear to be the largest source of bias in the ISCCP cloud amounts and that the accuracy of individual determinations of cloud cover depends on the size distribution of cloud elements. *Rossow et al.* [1993] found differences in total cloud amounts between ISCCP and surface observer reports over the tropical ocean to be less than 5% (on average) with ISCCP cloud fractions being somewhat larger (see Rossow et al.'s Table 3). When isolated to small broken cloud cases, however, they found ISSCP produced cloud fraction estimates that are too small

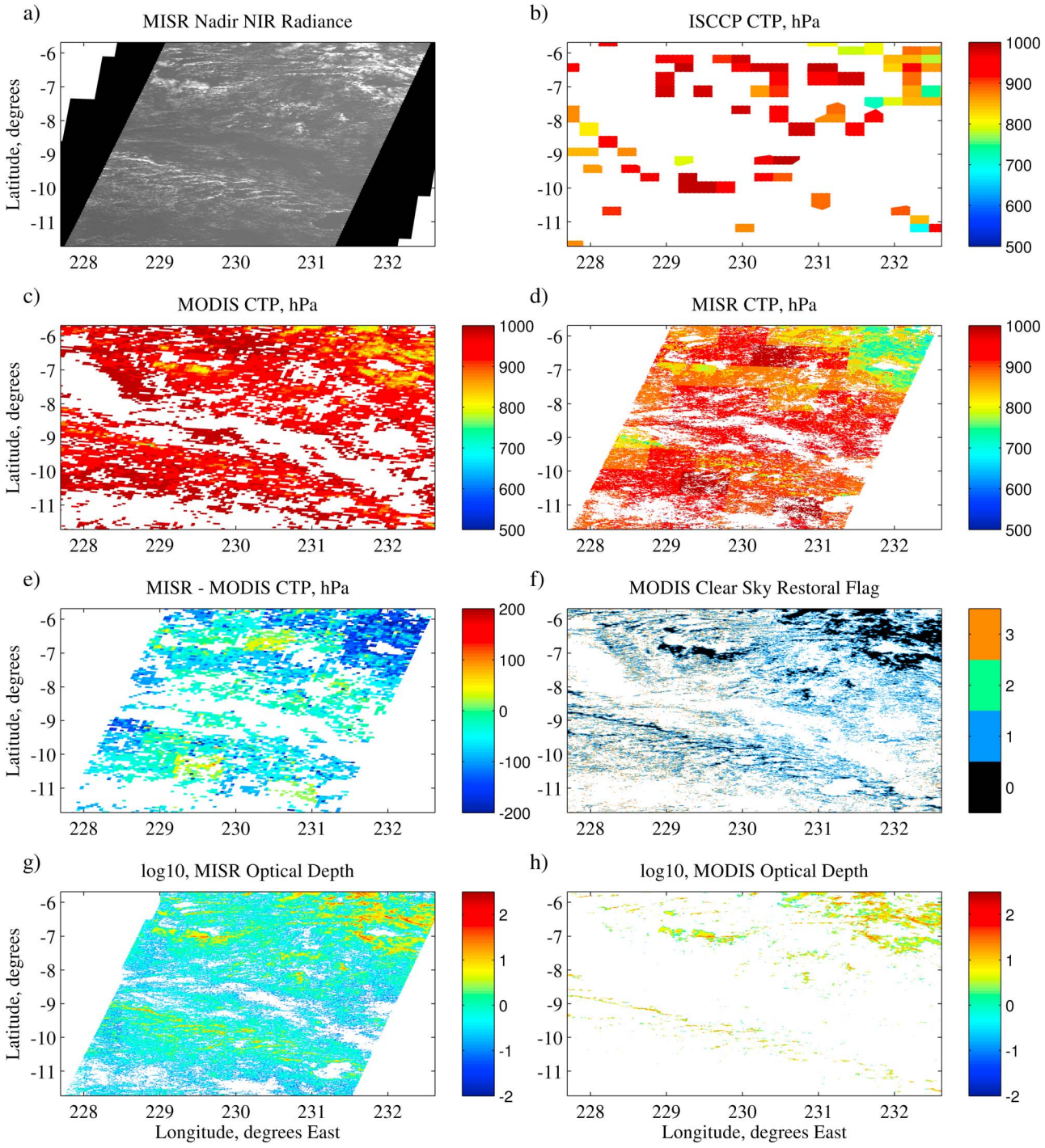

Figure 3. ISCCP, MODIS, and MISR retrievals for trade cumulus clouds observed on 25 April 2001 (MISR orbit number 7200). (a) MISR nadir view of cloud field at 865 nm, (b) ISCCP retrieved CTP, (c) MODIS (collection 5) retrieved CTP (5 km scale), (d) MISR retrieved height (converted into approximate pressure using NCEP reanalysis), (e) difference between MISR and MODIS CTP (where both retrieve a value), and (f) MODIS clear-sky restoral flag (value of 0 means cloud retrieval is attempted, other values indicate reason that pixel is treated as clear sky; see text for details). The combination of all categories in the image constitutes the 1 km MOD35 cloud mask. (g) MISR retrieved optical depth, and (h) MODIS retrieved optical depth.

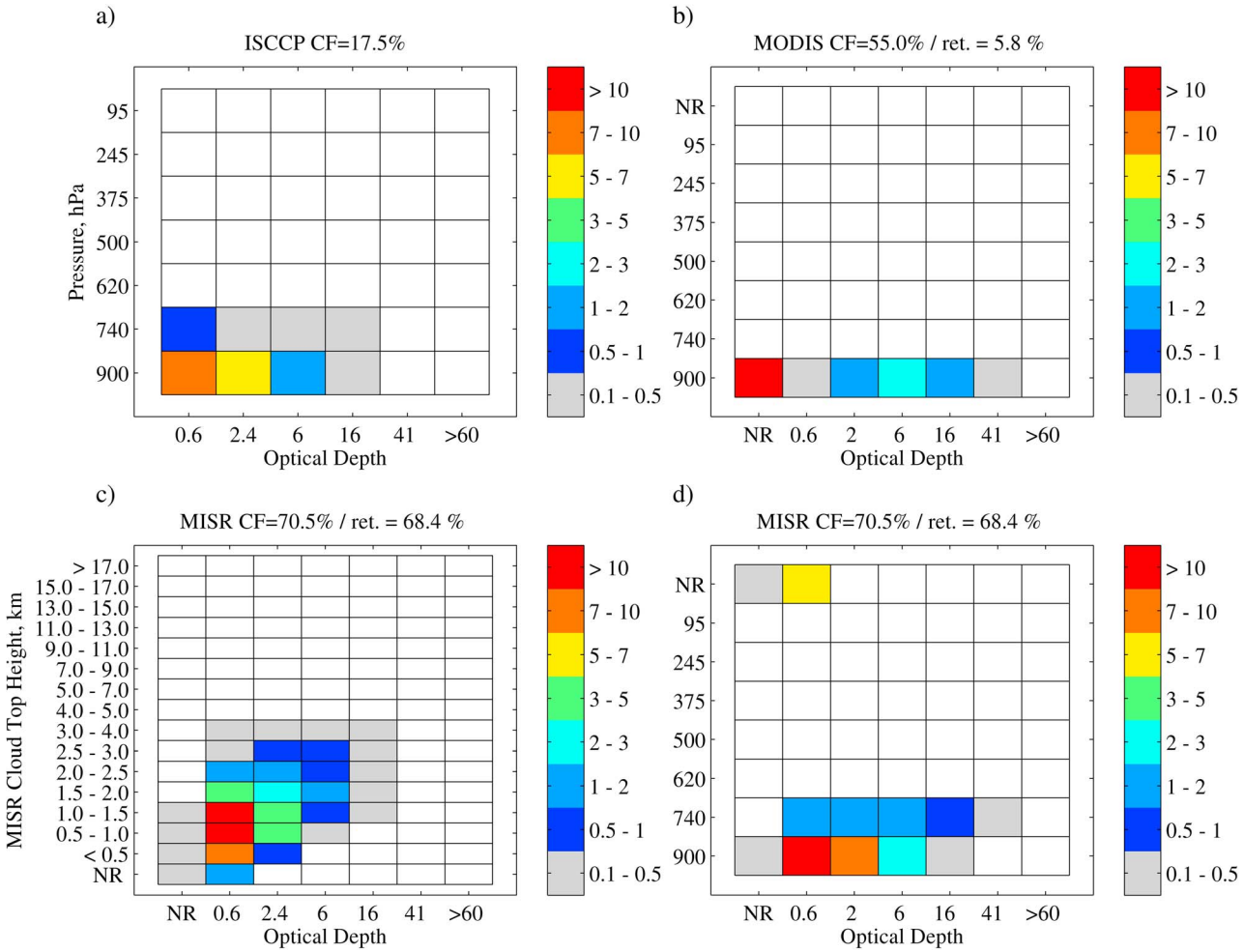

Figure 4. Joint histograms of cloud top height and optical depth for scene shown in Figure 3. Results for (a) ISCCP, (b) MODIS, (c) MISR, and (d) MISR mapped onto ISCCP/MODIS vertical pressure grid.

by about 4% (on average) and had a large root mean square uncertainty of 25%. Because one expects that some imager pixels will be partially cloudy, the fraction of pixels that contain at least some cloud should be larger than the true area covered by clouds. We will discuss this further in section 5. As the comparison here makes clear, ISCCP does not detect as much small trade cumulus as either MODIS or MISR. The scene examined here represents a particularly striking (or worse case) example with many small cloud elements (many barely detectable in the MISR 275 m imagery; see Figure 3a). On monthly or regional scales, Rossow et al. suggest a resulting root mean square uncertainty (and bias) of less than 10% for this cloud type. While we consistently find that ISCCP detects less cloud in areas with small broken clouds (at all latitudes, not just for tropical trade cumulus), we will show later that on a zonally averaged basis, the difference between ISCCP and MISR is about 10% or less.

[21] Figures 3g and 3h show the MISR and MODIS cloud optical depth retrievals. The MISR optical depth retrieval only fails when the observed 865 nm radiances are less than the estimated surface contribution. This can occur because the MISR radiometric cloud mask includes a spatial heterogeneity test, which causes relatively dark pixels (such as cloud shadows, for example) to sometimes be flagged as clouds. In general, failures of the stereo-height retrieval are more common. For this scene the height retrieval was unsuccessful for a little over 6% of the total pixels while the optical depth retrieval failed for only 0.5% of the pixels. MODIS, which simultaneously determines both the cloud optical depth and effective radius, does not process a significant number of pixels that were flagged as cloudy by the MOD35 cloud mask (categories 1–3 in Figure 3f). As mentioned in section 2, the MODIS retrieval is not applied to pixels on the edge of a MOD35 cloud (category 1 in Figure 3f) or partly cloudy pixel in the 250 m cloud mask (category 3). Figure 3f shows that edge pixels comprise a large percentage of all cloudy pixel in this scene. For this particular scene, only 5.8% of the MODIS pixels (relative to the total pixels) have an optical depth retrieval. The clouds with a MODIS optical depth retrieval are generally more reflective and appear to have higher cloud tops (as determined by MISR) than the clouds without a MODIS optical depth (see Figures 3a and 3e). The tendency for the brighter clouds to have higher cloud tops is captured in the MISR CTH-OD histogram (Figure 4c) which uses 500 m vertical

bins near the surface. This appears to be a general characteristic of trade cumulus [*Zhao and Di Girolamo*, 2007].

[22] The retention of optical depths by the MISR and ISCCP project for these broken cloud fields should not be taken to imply that the MISR or ISCCP retrievals have accurately retrieved the true optical depth of these clouds. The scattering of visible light by these clouds is fundamentally three-dimensional and satellite retrievals based on one-dimensional theory will not generally yield accurate results [see, e.g., *Evans et al.*, 2008]. As such, the counts (or cloud fractions) in the low-optical depth region of the MISR and ISCCP histograms often denote the presence of partially filled pixels and the retrieved optical depth is perhaps best regarded as 1D equivalent optical depth (at a scale of one to a few km).

3.3. Thin Cirrus and Multilayer Clouds

[23] Optically thin cirrus and multilayer clouds involving such cirrus are common and often challenging for satellite retrievals. Figure 5 shows an example of this cloud type observed on May 10, 2001 (MISR orbit 7433, MODIS overpass 1900 UTC). Figures 5a and 5b show the MISR 865 nm reflectance from the MISR nadir and 60° forward viewing cameras, respectively. Figures 5a and 5b reveal a scene covered by a horizontally extensive cirrus cloud. While the 865 nm reflectance varies over the scene, most of the cirrus cloud is transparent enough that low-level clouds are easily observed beneath the cirrus, especially in the lower third of the image where a weak convergence line is visible. The MISR 60° forward view more clearly reveals the cirrus cloud, because the cirrus cloud preferentially forward scatters solar photons in this direction and because photons reflected from the surface or lower clouds must travel twice the distance through the cirrus cloud (twice the path length), which decreases the likelihood they can reach the satellite without being redirected by the cirrus cloud. Figures 5c, 5e, and 5f show the associated ISCCP, MODIS, and MISR cloud top height retrieval. Figure 5d shows the ISCCP cloud top height prior to the application of the "visible adjustment" portion of the ISCCP algorithm, which we will describe in more detail below, and Figure 5g shows the difference between the MISR and MODIS retrieved cloud top pressures.

[24] In Figures 5c–5f, the red rectangle highlights the location of a multilayer cloud region in which the ISCCP, MODIS, and MISR cloud top height retrievals produce starkly differing results. Because the MISR stereo-imaging retrieval is based on pattern matching in multiple views, the MISR retrieval preferentially returns the height of the low-level clouds (whose reflectance varies more strongly than the cirrus cloud at 275 m resolution and thereby generates a strong pattern). The CO_2 technique used by MODIS, on the other hand, is sensitive to subtle differences in the cirrus cloud infrared transmittance/emission (rather than the location from which most of the visible wavelength photons are reflected back toward space) and the MODIS retrieval is able to estimate the height of the upper cirrus cloud. Within the red rectangle, in only one small area is the cirrus sufficiently thin that the MODIS CO_2 slicing retrieval doesn't succeed and the MODIS algorithm switches to the simpler (ISCCP-like) single-channel brightness temperature technique. For this same area, the ISCCP retrieval produces a cloud top pressure largely between 500 and 600 hPa (an altitude between the cloud layers where it is unlikely that any actual cloud condensate exists). It has long been understood that both the single-channel brightness temperature technique and the CO_2 slicing technique can produce cloud top pressures that are too large in multilayer cloud situations when the upper-level cloud is sufficiently thin that it does not radiate like a thermal blackbody (that is, it has an emissivity significantly less than one) and the observed infrared temperature is increased by emissions from the surface or lower clouds which penetrate the upper-level cloud [*Baum and Wielicki*, 1994; *Jin and Rossow*, 1997; *Stubenrauch et al.*, 1999; *Rossow et al.*, 2005]. In both the ISCCP and MODIS retrievals, clouds are effectively assumed to be single layered and in multilayer cases the retrieved cloud top pressure responds to the radiative mean between the two cloud layers. As this example shows, the effect is much larger in the single-channel brightness temperature approach than with the CO_2 slicing approach, which depends on measurements in two infrared channels. A similar result was found by *Holz et al.* [2008] when comparing MODIS retrieved cloud top pressures with spaceborne lidar observations (from CALIPSO). Nonetheless, the MODIS retrieval does produce some cloud top pressures between the two layers even when the MODIS CTP retrieval flag indicates that the CO_2 retrieval technique was used in the retrieval. This often occurs in the vicinity of transitions where MODIS switches between the CO_2 retrieval technique and the single-channel brightness temperature technique. In the current scene, this is most noticeable around the edges of the low clouds in the top left corner of Figure 5e (where the cirrus appears to be patchy and thin) and may well be a result of averaging of the MODIS 1 km observations (at nadir) to a 5 km (5 × 5 pixel) grid prior to running the cloud top pressure retrieval [*Menzel el al*., 2008]. This effect was much less evident in the earlier MODIS collection 4 retrievals where such averaging was not used (not shown). While the differing responses of the ISCCP, MODIS, and MISR retrievals to multilayer clouds complicate comparisons of these data with model output, the differences also provide insight into the relative importance of these clouds. As we demonstrate in section 4, we can take advantage of the differences between the data sets to characterize the amount of multilayer cloud.

[25] For single-layer cirrus, ISCCP, MODIS, and MISR appear to have roughly similar detection limits with estimates for the minimum detectable optical depth (at visible wavelengths) varying between about 0.1 and 0.4 [*Ackerman et al.*, 2008; *Dessler and Yang*, 2003; *Marchand et al.*, 2007; *Rossow and Schiffer*, 1999; *Whiteman et al.*, 2001]. The detection is generally better over dark water surfaces than land surfaces. In a comparison of the MODIS cloud mask with airborne high spectral resolution lidar observations, *Ackerman et al.* [2008] found that 60% of failed detections occur when the cloud optical depth was less than 0.2, and 90% of the failed detections occur when the cloud optical depth was less than 0.4. Figure 5g plots the difference between the MISR and MODIS retrieved cloud top pressure. In areas with single-layer cirrus, the MISR and MODIS retrievals largely agree to within 50 hPA (roughly equivalent to 1.5 km at this attitude). While in some areas the MISR cloud top pressure is larger than MODIS (e.g.,

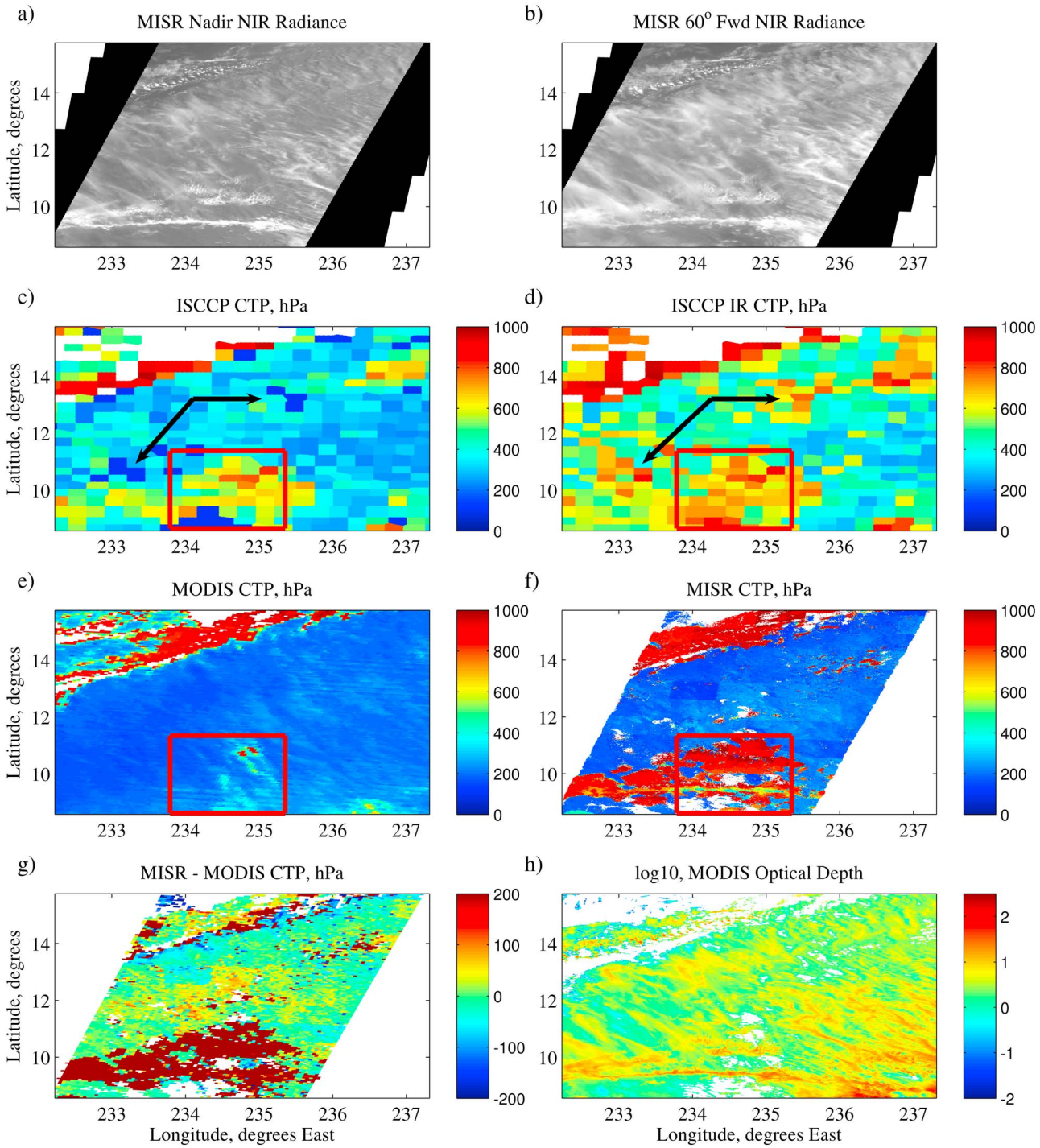

Figure 5. ISCCP, MODIS, and MISR retrievals for a multilayer cloud scene. (a) MISR nadir view of cloud field at 865 nm, (b) MISR 60° aft view, (c) ISCCP retrieved CTP, (d) ISCCP retrieved CTP before visible adjustment, (e) MODIS (collection 5) retrieved CTP, and (f) MISR retrieved height (converted into approximate pressure using NCEP reanalysis). (g) Difference between MISR and MODIS retrieval of CTP, and (h) MODIS retrieved optical depth (collection 5). The red rectangle denotes an area with primarily multilayer cloud, while black arrows indicate the location of pixels whose height has been assigned to the tropopause (see text).

throughout much of the center of the scene), in other areas the MISR cloud top pressure is smaller. Whether MODIS or MISR retrieves a higher cloud top appears to involve a variety of factors including the accuracy of the MISR wind correction, as well as the physical and optical thickness of the cirrus layer and the vertical distribution of extinction. The lack of a wind correction can result in MISR retrieving either a higher or lower cloud top depending on the wind

direction. In a comparison of MISR and MODIS heights with ground based cloud radar at two sites, *Naud et al.* [2005] found that MISR and MODIS cloud pressures (for high-altitude clouds) usually agreed to within 1 km with an average difference between the two of 200 m. Both MISR and MODIS cloud top retrievals tend to be located below true cloud top for "diffuse" topped clouds [*Frey et al.*, 1999; *Marchand et al.*, 2007; *Menzel et al.*, 2008; *Naud et al.*, 2002, 2004, 2005]. *Marchand et al.* [2007] found MISR cloud top heights tend to be located within the volume filled by cloud (rather than true cloud top), typically 500 to 1500 m below true cloud top (as identified by cloud radar or lidar) often near the level where the cloud optical depth reaches 1 to 2 (when the cloud optical depth exceeds one). For single-layer clouds, the same is true of MODIS cloud top heights [*Menzel et al.*, 2008; *Holz et al.*, 2008].

[26] For single-layer cirrus, the ISCCP cloud top pressure is generally a bit higher (cloud top is slightly lower in altitude) than either the MISR or MODIS retrievals, but there are a few ISCCP pixels where the cloud top pressure is notably lower (cloud top is much higher in altitude). Black arrows in Figure 5c identify several pixels where ISCCP indicates very low cloud top pressures. This combination of pixels with both low and high cloud top biases occur because the cirrus cloud emissivity is less than one and the observed ISCCP infrared brightness temperature is larger than it would be if the cirrus cloud was a blackbody (that is, larger than the temperature of the atmosphere at the altitude where the cirrus is located). The ISCCP retrieval algorithm must therefore correct for the emission through such thin cloud. It does so by approximating the cloud optical depth in the infrared from the retrieved optical depth at visible wavelengths and then estimating the contribution of the surface emission to the observed brightness temperature. This correction is known as the visible adjustment and is important because a large fraction of all high clouds have an emissivity significantly less than one. Figure 5d shows the ISCCP retrieved cloud top pressure prior to the visible adjustment. Comparing Figures 5c and 5d shows that the visible adjustment produces a large change in the retrieved cloud top pressure in the areas covered by only the single-layer cloud, but little difference for the multilayer cloud in the area highlighted by the red rectangle. In the multilayer region the lower cloud visible reflectance is large compared with the thin upper-level cloud. This results in a relatively large optical depth and no significant change in the retrieved cloud top pressure because the algorithm depends on the total column optical depth, essentially falsely assuming a single-layer cloud, and the cloud appears to be too thick for the surface to have significantly influenced the observed temperature. In the single-layer cirrus region, the visible adjustment procedure produces a large improvement in the retrieved cloud top pressure though the correction often appears to be too small (retrieved cloud top remains too low in altitude). In comparison with retrievals from the Stratospheric Aerosol and Gas Experiment II (SAGE II) satellite (a limb viewing sensor), *Liao et al.* [1995] determined that clouds with "diffuse cloud tops" are encountered above 440 hPA level almost 70% of the time in the tropics, with ISCCP retrieving a "radiative" cloud top pressure that is 150 hPA too large on average, and about 30–40% of the time at higher latitudes with an average discrepancy of about 50 hPA. In a few pixels, however, the adjustment appears to have been much too large (see black arrows). In these pixels, ISCCP detects the cloudy based on its IR threshold while the visible reflectance is very close to the expected clear-sky value. In this situation, ISCCP is generally unable to accurately determine the optical depth. As a result, the ISCCP algorithm assigns the cloud top temperature to the expected tropopause temperature minus 5 K (with a resulting cloud top pressure near the tropopause).

[27] Figure 6 shows the resulting joint histograms of cloud top height and optical depth for the scene shown in Figure 5. As one would expect from the above discussion, ISCCP (Figure 6a) falsely identifies more midlevel cloud than either MODIS (Figure 6b) or MISR (Figure 6c). This includes most of the cloud with optical depths larger than 10 (multilayer clouds). In the ISCCP thinnest optical depth column (0–1.3), the clouds tend to be either biased low or have been assigned to the lowest pressure bin (the upper left corner of the CTP-OD histogram). MODIS and MISR place the cirrus at about the same altitude, with MISR identifying much more low cloud. Unlike the case for broken boundary layer clouds (Figures 3 and 4), MODIS successfully retrieves an optical depth for most of the thin cirrus (see Figure 5h), although about 10% of the optically thinnest cloud (identified in the MODIS MOD35 cloud mask) is still not included. The impact of the missing MODIS retrievals on the distribution of cloud optical depth is highlighted in Figure 6e, which shows that the MODIS histograms contain somewhat less optically thin cloud relative to ISCCP or MISR. While potentially significant, the amount of missing thin cloud is much smaller for high clouds than low-level clouds (see section 3.2). There are also some areas (about 6% of the pixels) where the MISR stereo height retrieval is not successful (these pixels are shown in white in Figure 5f). These missing patches seem to have little impact on the overall MISR cloud top height or optical depth distributions. While MISR sometimes fails to retrieve a CTH because a cloud is unusually featureless (and no stereo matching is possible) more often (as is the case here) it fails in geometrically complex regions adjacent to multilayer clouds. The distributions of the cirrus cloud properties in the missing areas tend to be similar to the retrieved areas (that is, the cirrus appear to be randomly overlapped with the low cloud) and so the estimated distributions are largely unaffected.

4. Comparison of ISCCP, MODIS, and MISR CTH-OD Histograms

[28] Following ISCCP, the MODIS and MISR projects have created simple global summaries of cloud top heights and optical depths by constructing two-dimensional (or joint) histograms of these two retrieved quantities. In this section, we examine the ISCCP D2, MODIS MOD08, and MISR CTH-OD global data sets for 2001. We begin with the North Pacific, and follow this with discussion of the global distributions of total and low-level cloud occurrence, midlevel and multilayer cloud occurrence, and finally end with high altitude clouds and the tropical western Pacific.

4.1. North Pacific

[29] Figures 7a, 7b and 7c shows the joint histograms of cloud top height and optical depth produced by ISCCP,

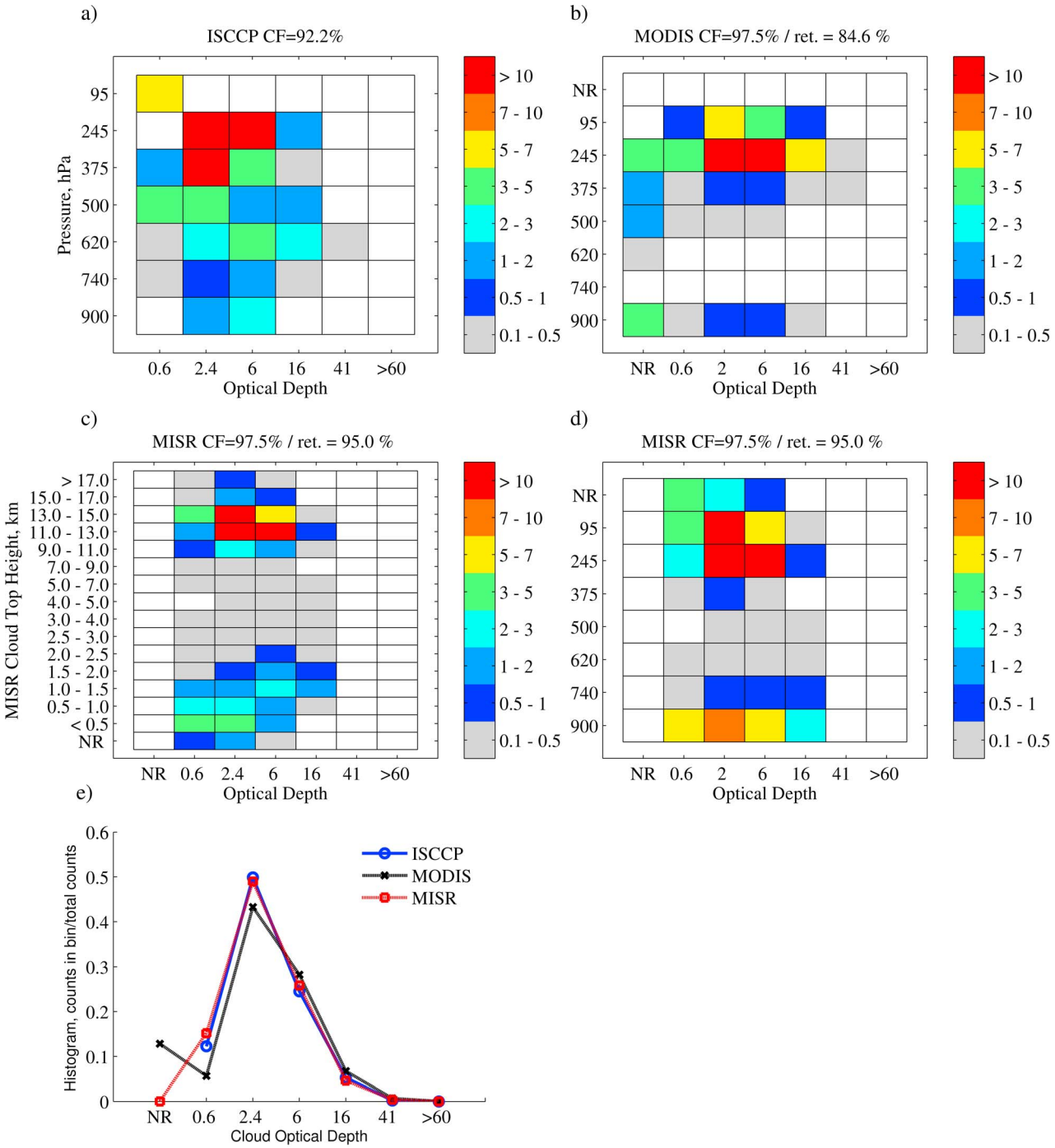

Figure 6. Joint histograms of cloud top height and optical depth for scene shown in Figure 5. (a–d) Same as Figures 4a–4d. (e) Comparison of the distribution of cloud optical depth for all three data sets.

MODIS, and MISR, respectively, for the North Pacific (30° to 60° N, 140° W to 160° E) for 2001. The MISR operational histograms (Figure 7c) use 16 height bins, giving a somewhat more detailed picture of the vertical structure. To facilitate comparisons among the projects, in Figure 7d we have mapped the MISR histogram on to the pressure grid used by ISCCP and MODIS (using monthly averaged NCEP reanalysis pressure profiles for this region and assuming cloud tops are uniformly distributed in each MISR height bin when a MISR height bin straddles a pressure bin boundary). The MOD08 product also has finer bin resolution product (not shown). All three projects use basically the same optical depth bin boundaries, although the MISR and MODIS projects have divided the first optical depth bin used by ISCCP (0.02 to 1.3) into two bins (0 to 0.3 and 0.3 to 1.3) to facilitate comparison with models, because all three satellites frequently fail to detect clouds with optical depths smaller than about 0.3. A description of all bin

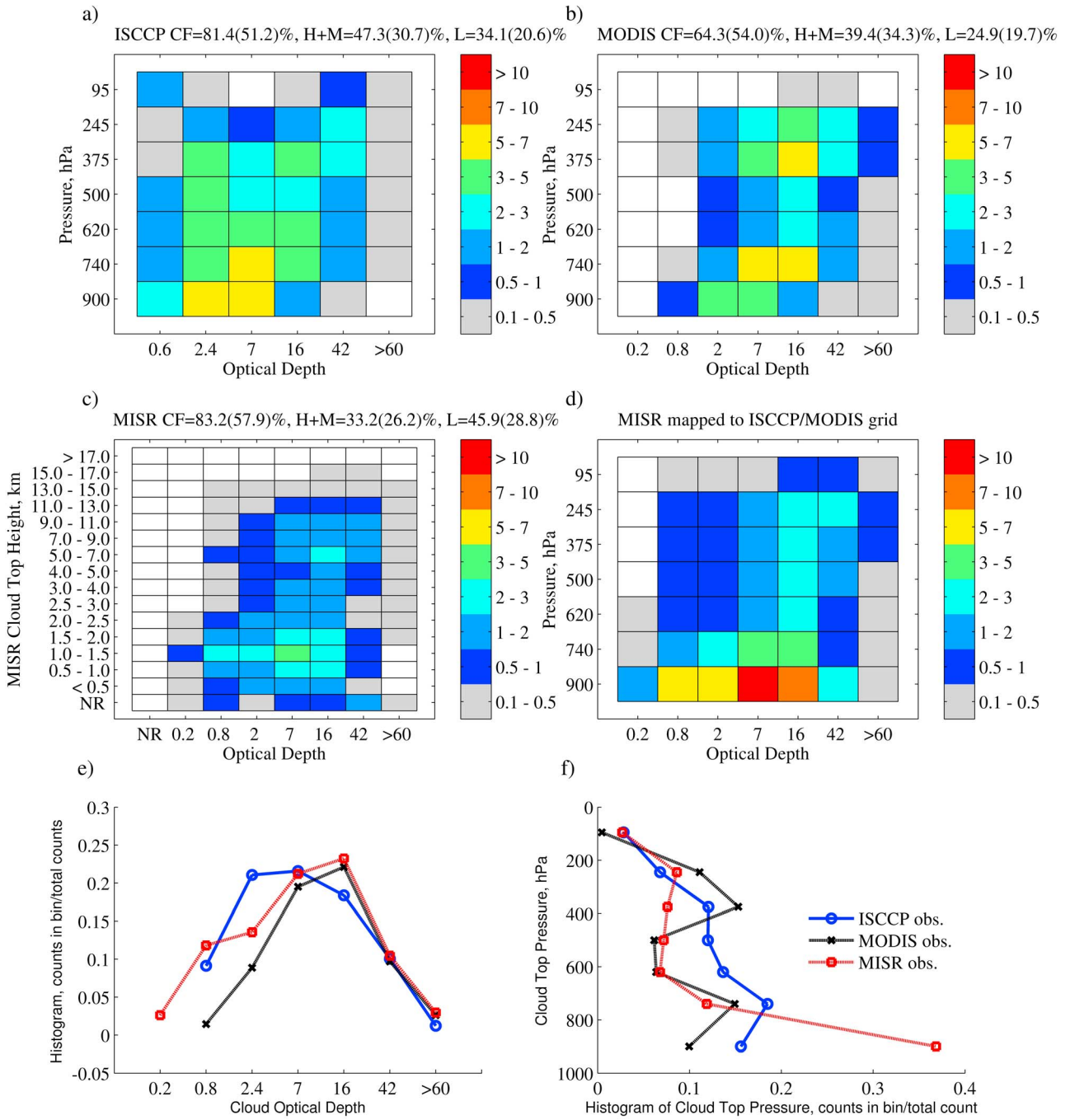

Figure 7. Joint histograms of cloud top height and optical depth from (a) ISCCP, (b) MODIS, and (c) MISR for the North Pacific in 2001. (d) MISR result mapped onto the MODIS/ISCCP vertical pressure grid. (e) Comparison of the distributions of cloud optical depth (for cloud with tops at all heights) from the three projects, and (f) comparison of the distribution of cloud top heights.

boundaries is given in Tables 1a–1c. The MISR operational histograms also contain a no-retrieval (NR) bin (on each axis) to represent those cases where a cloud is detected by the MISR radiometric cloud mask but either no optical depth was retrieved or no cloud top was retrieved. This feature is not included in the MODIS operational histograms. In Figures 7a, 7b and 7c the total retrieval cloud fraction for each data set is listed at the top. The total fraction (cloud top at any height) as well as the fraction of High + Middle (H/M) cloud (pressure < 680 hPA) and Low (L) cloud (pressure > 680 hPa) is given. The total fraction in each category is listed first, with the fraction having an optical depth above 9.4 given in parentheses. In addition, Figure 7e compares the distributions of cloud optical depth (for clouds with cloud tops at any altitude) for all three data sets and Figure 7f compares the distributions of cloud top pressure. The

Table 1a. Joint Histogram Bin Ranges for Optical Depth Bins[a]

	Bin Number						
	1	2	3	4	5	6	7
Optical depth	0–0.3	0.3–1.3	1.3–3.6	3.6–9.4	9.4–23	23–60	>60

[a]ISCCP uses 1 less bin, with the first bin optical depth range from 0.02–1.3. MISR histograms also contain an "NR" (No Retrieval) bin which indicates how often cloud is identified by the radiometric cloud mask but the optical-depth retrieval was unsuccessful.

MODIS and MISR cloud fractions and profiles (Figure 7f) do not include the small percentage of clouds with optical depths less than 0.3.

[30] While the histograms for all three projects show some similarities (for example, they all indicate the presence of a high-altitude optically thick cloud mode and a low-altitude cloud mode), they also show distinct differences. Figure 7f shows that MISR identifies significantly more low-altitude cloud (cloud top pressure > 680 hPA) than ISCCP or MODIS, while ISCCP identifies more midlevel cloud (cloud top pressure between 680 and 440 hPA), and MODIS identifies more high cloud (cloud top pressures above 400 hPA). As demonstrated in section 3, this characteristic is consistent with the response of the satellite retrievals to multilayer clouds where the upper layer is optically thin; ISCCP retrieves a cloud top height that is frequently biased into midlevels, whereas MODIS usually identifies the upper-level cloud and MISR the lower cloud top. We can use the fact that MISR preferentially "sees" through the thin upper-level cloud to make an estimate for the amount of such multilayer cloud. Subtracting the fraction of high-level + midlevel cloud determined by ISCCP (~48%) from the fraction of high-level + midlevel cloud found by MISR (~33%), suggests that 15% of the time clouds in the North Pacific are multilayered with a low-level cloud and an upper layer that is thin enough for MISR to "see" through (and thick enough for ISCCP to detect). Based on an analysis of MISR stereo heights with radar and lidar retrievals, *Marchand et al.* [2007] found that the upper cloud must typically have an optical depth less than about 1 to 2 for this to occur.

[31] This estimate is approximate for a variety of reasons including: (1) ISCCP and MISR data sets are based on entirely different satellite platforms with different temporal sampling, (2) it assumes that ISCCP and MISR can both detect roughly the same amount of single-layer cirrus, and (3) the estimate may be in error if ISCCP overestimates the altitude of low clouds (biasing them into midlevels). With regard to the first concern, we calculated the multilayer cloud amount using the monthly ISCCP D1 3-hourly average (taking the data closest in time to the MISR overpass) rather than the ISCCP D2 data set that averages data from all daylight hours. The difference for the North Pacific was less than 1% percent, and on a zonally averaged basis only at high latitudes (above about 60°) were the differences more than 3% percent. (The ISCCP D2 data set is used for all discussion and plots in this section). With regard to the second concern, several studies have found the minimum detectable optical depth at visible wavelengths for both ISCCP and MISR to be between about 0.1 and 0.4, with detection over water being somewhat better, between about 0.1 and 0.2 [*Marchand et al.*, 2007; *Rossow and Schiffer*, 1999; *Whiteman et al.*, 2001]. We also note that in the North Pacific, ISCCP and MISR see about the same total cloud cover with MISR detecting clouds 83% of the time and ISCCP detecting clouds 82% of the time. This agreement is only likely to happen if ISCCP and MISR are about equally sensitive single-layer high-level and midlevel clouds. In principal one data set could be less sensitive to single-layered high-level and midlevel clouds but compensate by finding more low-level clouds. This may be true to a small degree, however, if we estimate the amount of single-layer low cloud in the MISR data set as the total amount of low cloud detected by MISR (46%) minus the estimated amount of multilayer layer cloud (15%) we obtain 31%, which compares well with the total amount of low cloud found by ISCCP at 34%. (As we will discuss later, it is likely that ISCCP detects slightly more single-layer thin cirrus than MISR in the tropics, which will likely cause a small overestimate in the amount of multilayer cloud in this region.) The third concern, that ISCCP sometimes overestimates the height of low clouds, also does not appear to be a problem in the North Pacific, as evidenced by the similar amounts of low cloud identified by the two data sets. However, as we will discuss later in this section, this is a significant problem off the west coast of South America.

[32] The MODIS Level 3 product (which only includes successful optical depth retrievals) contains less total cloud (~64%) compared with ISCCP or MISR (both just over 80%). Figure 7e shows that the difference is largely due to the MODIS histogram containing less optically thin cloud. Based on the case studies presented in previous section, this is an expected result for both broken low clouds and

Table 1b. Joint Histogram Bin Ranges for ISCCP and MODIS Cloud Top Pressure Bins

Bin Number	Cloud-Top-Pressure Range
1	0 – 180 hPA
2	180 – 310 hPA
3	310 – 440 hPA
4	440 – 560 hPA
5	560 – 680 hPA
6	680 – 800 hPA
7	> 800 hPA

Table 1c. Joint Histogram Bin Ranges for MISR Cloud Top Height Bins

Bin Number	Cloud-Top-Height Range
1	No retrieval
2	0–0.5 km
3	0.5–1.0 km
4	1.0–1.5 km
5	1.5–2.0 km
6	2.0–2.5 km
7	2.5–3.0 km
8	3.0–4.0 km
9	4.0–5.0 km
10	5.0–7.0 km
11	7.0–9.0 km
12	9.0–11.0 km
13	11.0–13.0 km
14	13.0–15.0 km
15	15.0–17.0 km
16	>17 km

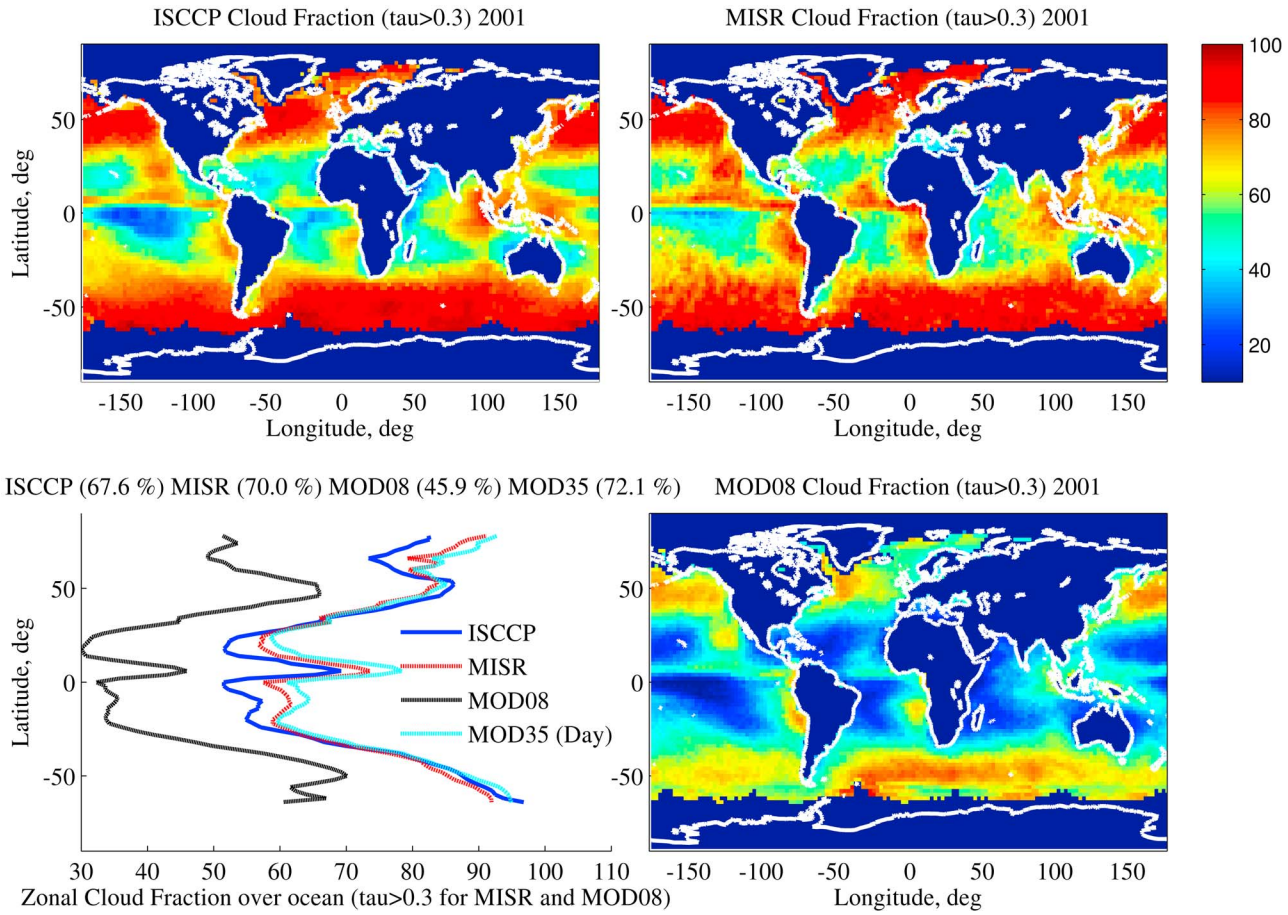

Figure 8. Total cloud cover for 2001 over ocean for (top left) ISCCP, and (top right) MISR, (bottom right) MODIS (MOD08) obtained from cloud top height and optical depth joint histogram data sets. MISR and MODIS (MOD08) plots include only clouds with optical depth > 0.3. (bottom left) Comparison of zonal averages (cosine weighted) with global averages shown above the plot. The light blue dashed line shows cloud fraction from MODIS operational cloud mask product (MOD35); see text.

optically thin high clouds (optical depths less than 1). We note that MISR and MODIS distributions of cloud optical depth are similar for clouds with optical depths larger than about 9.4, while the ISCCP distribution appears to be shifted toward lower values. We discuss the shift in the ISCCP distribution later in this section. Because MISR and MODIS both detect about the same amount of optically thick cloud and both detect optically thick high clouds well, we can estimate the amount of multilayer cloud (and single-layer low clouds) using MISR and MODIS using much the same approach applied to ISCCP and MISR earlier in this section, except restricted to the optically thick portion of the distribution. Subtracting the fraction of optically thick high-level + midlevel cloud determined by MODIS (~34%) from the fraction of optically thick high-level + midlevel cloud found by MISR (~26%), suggests that 8% of the time clouds in the North Pacific are multilayered with an upper layer that is thin enough for MISR to "see" through and the total column optical depth larger than about 9.4. Because the MODIS technique shows relatively little tendency to bias cloud tops into midlevel (unlike ISCCP), we can likewise estimate the amount of thin high cloud over midlevel cloud by subtracting the MODIS high-level cloud fraction (with optical depths larger than about 9.4) from the MISR high-level cloud fraction. For the North Pacific, this comes to about 3%.

[33] In summary, the ISCCP, MODIS, and MISR data sets tell us more about North Pacific clouds than any one data set on its own. The combination of ISCCP and MISR or MODIS and MISR enable one to estimate the amount of multilayer cloud with an optically thin upper-level cloud. Taken together these data indicate: (1) a total single-layer low cloud fraction with an optical depth greater than 0.3 of about 30%, with about 20% or 2/3 having an optical depth greater than 9.4; (2) a total combined high-level and mid-level cloud fraction with an optical depth greater than 0.3 of about 48%, with 34% or a little over 2/3 having a total column optical depth greater than 9.4; (3) a multilayer cloud fraction with low cloud below and optically thin high-level or midlevel cloud of about 15%, with a total column optical depth greater than 9.4 occurring about 8% of the time; and (4) a multilayer cloud fraction with midlevel cloud below and optically thin high and a total column optical depth greater than 9.4 of about 3%.

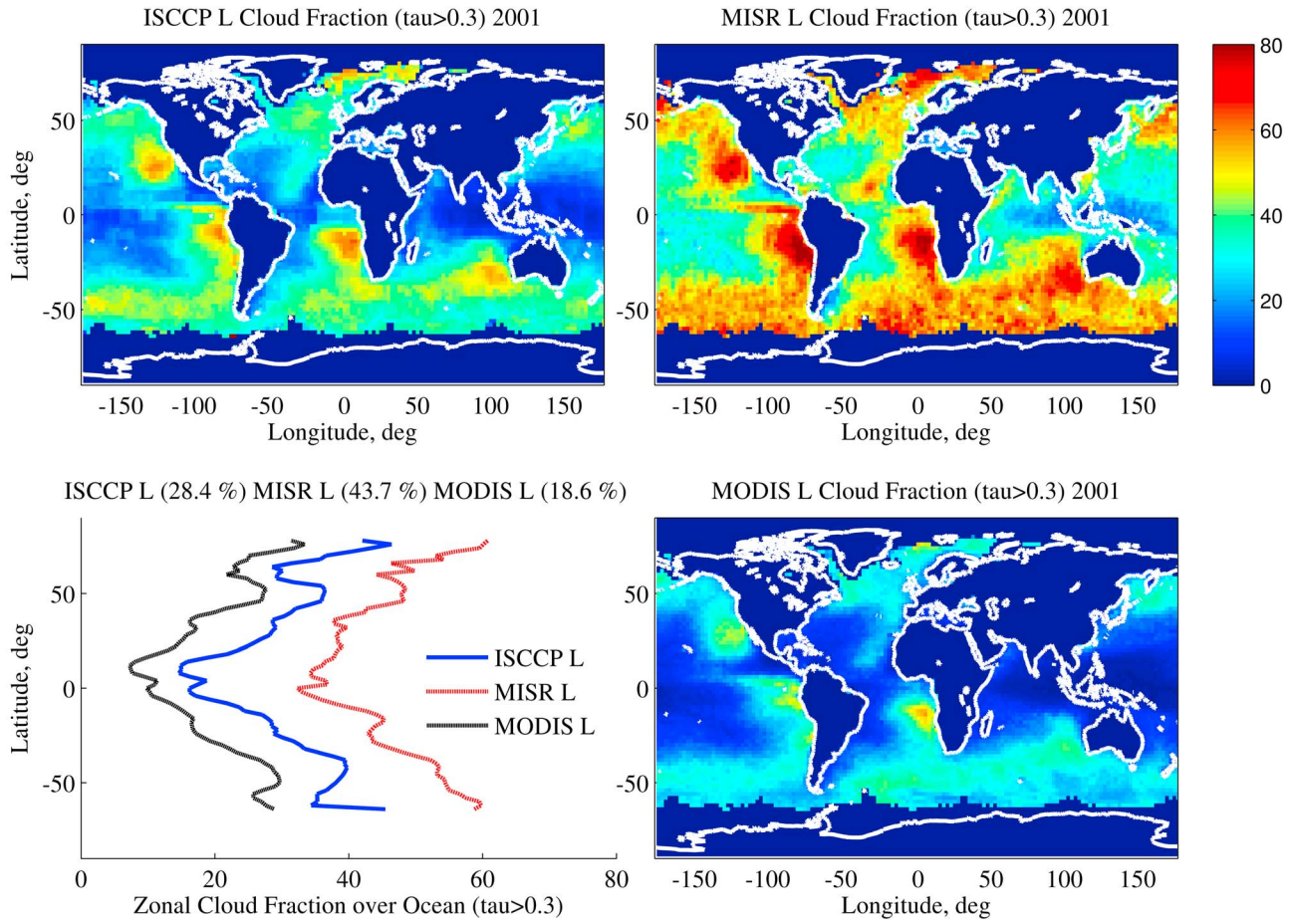

Figure 9. Low (L) cloud cover over ocean (cloud top pressure > 680 hPA) average for 2001 for (top left) ISCCP, (top right) MISR, and (bottom right) MODIS obtained from cloud top height and optical depth joint histogram data sets. (bottom left) Comparison of zonal averages with the global (cosine weighted) average shown above the plot.

4.2. Global Distribution of Total and Low-Level Clouds

[34] Many of the differences among the ISCCP, MODIS and MISR data sets examined for the North Pacific are characteristic over most oceanic regions. Figure 8 shows the total cloud (retrieval) fraction (with cloud tops at any altitude) in the ISCCP, MISR and MODIS (MOD08) CTH-OD data sets over ice-free ocean. The MODIS and MISR histograms are compiled on a simple fixed latitude and longitude grid. The ISCCP histograms are stored on a fixed area grid and have been interpolated onto a fixed latitude and longitude grid (using a "nearest neighbor" approach) in Figure 8 and Figures 9–13 shown in this section. Figure 8 (bottom left) shows that, zonally averaged, the MISR and ISCCP joint histograms contain very similar total cloud amounts, especially in midlatitudes. In the tropics, subtropics and latitudes poleward of about 55° (in both hemispheres), the MISR data set has slightly more total cloud. This is due to MISR detecting more low (L) cloud and more single-layer low cloud (L*), as shown in Figures 9 and 10, respectively. The MISR single-layer low cloud (L*) is calculated as the total MISR low cloud fraction (L) minus the estimated amount of multilayer cloud, which we discuss further later in this section. Based on case study analysis, the increase in MISR low cloud amount is likely due to MISR detecting a much larger percentage of small or partially filled (subpixel clouds) in broken cloud conditions. In the subtropics and tropics, the difference approaches 10% (zonally averaged).

[35] As expected, Figure 9 (bottom) shows that the MODIS (MOD08) joint histogram contains significantly less total cloud (fewer retrievals) than MISR or ISCCP primarily because optical depth retrievals are including only those cloudy elements which are not edge pixels (see section 3.2) but also because optical depth retrievals are not attempted for very optically thin cirrus cloud (see section 3.3). Figure 10 (bottom) shows that the later restriction has a large effect on the amount of low-level cloud in the MOD08 CTP-OD histograms. The MODIS operational cloud mask (MOD35) detects a roughly similar amount of total cloud to MISR, as shown by the light blue line in Figure 8 (bottom left). The MOD35 cloud fraction includes all cloud detections, including those clouds whose retrieved optical depth would likely be less than 0.3. However, as was observed in the North Pacific data, the MODIS and MISR total cloud fractions for clouds with optical depths larger than about 9.4 are very similar in most regions (see Figure 11). Interestingly, the MODIS and MISR cloud fractions for cloud with optical

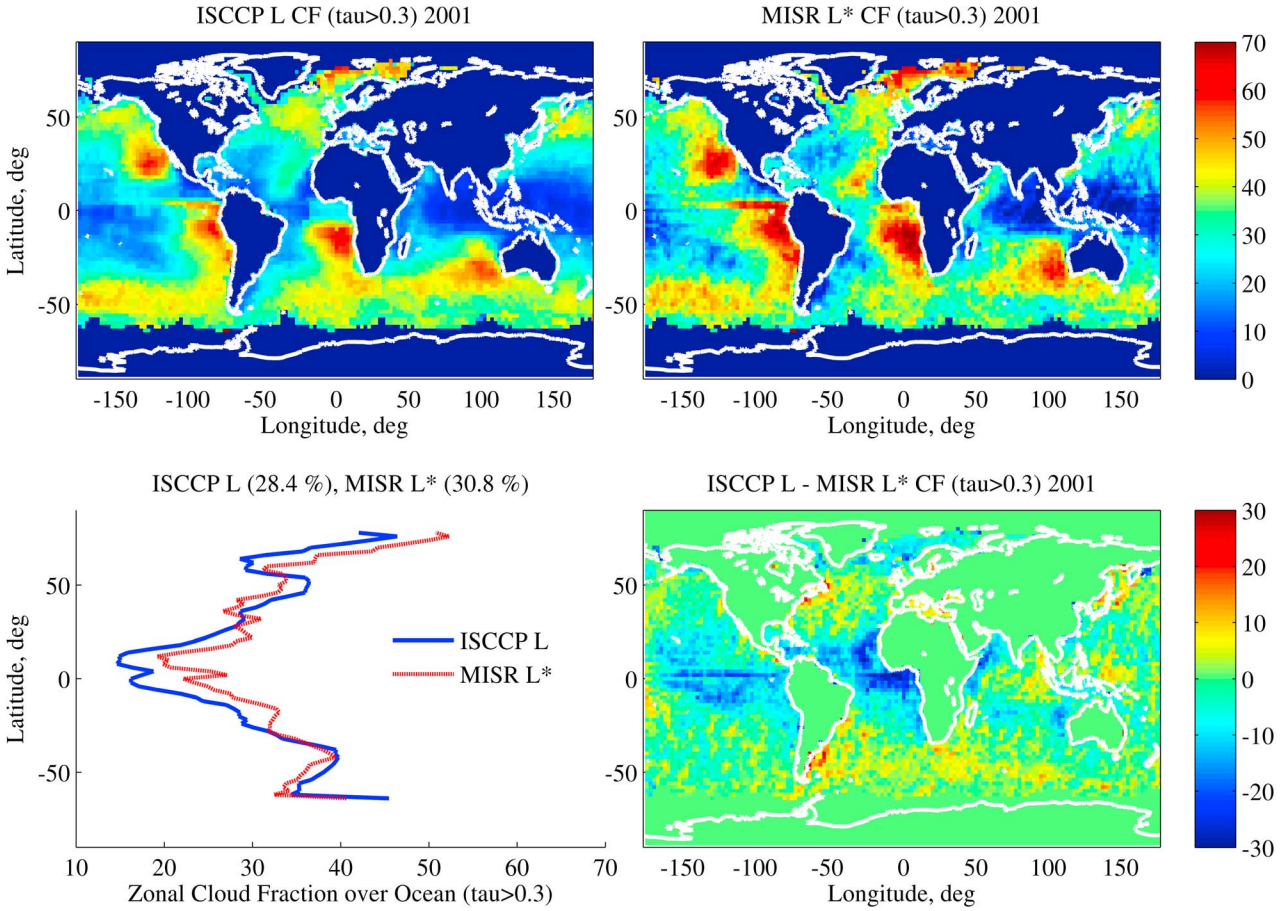

Figure 10. Comparisons of ISCCP Low (L) cloud cover over ocean (cloud top pressure > 680 hPA) with estimate of single-layer low (L*) cloud cover from MISR (average for 2001). (top left) ISCCP, (top right) MISR, and (bottom right) difference plot (ISCCP-MISR). MISR L* = MISR L – estimated multilayer cloud amount (see text and Figure 12). (bottom left) Comparison of zonal averages with the global (cosine weighted) average shown above the plot.

depths larger than 9.4 differ slightly poleward of about 50° latitude in both hemispheres (see Figure 11, bottom left). In our case study evaluations we found no cases (including cases poleward of 50° latitude) where the MODIS and MISR histograms differed in this way. However, our case study analysis was restricted to examining MODIS data only on that part of the swath where MISR data exists. The MISR swath width is about 400 km, which is much narrower than the MODIS swath width of about 2300 km. The wider MODIS swath means that MODIS observes regions more frequently (at different times of day), at a wider range of solar zenith and view zenith angles and with lower resolution (larger pixel sizes) much of the time. However, other factors such as unrecognized sea ice may also play a role in this difference. More research will be needed to determine the exact cause. Whatever the cause, the similarity of the results equatorward of 50° suggest that the MISR and MODIS (optical depth > 9.4) cloud fractions are likely accurate to a few percent at these latitudes (over ocean), while the difference poleward of 50° suggest that comparison of these data with model output should consider them more uncertain (roughly ~5 to 10%).

[36] With regard to the ISCCP distribution of cloud with optical depths greater than 9.4, Figure 11 (top) shows that on an annually averaged basis ISCCP detects a similar amount of optically thick cloud in the tropics and subtropics to that found by MISR and MODIS, but somewhat less cloud at midlatitudes (and, to some extent, high latitudes), especially in the Southern Hemisphere. The ISCCP data combines observations from both geostationary weather satellites and polar orbiting satellites (AVHRR), with geostationary weather satellites contributing a large fraction of the data at midlatitudes and low latitudes. Because geostationary satellites hover near the equator, the resolution of most of the ISCCP retrievals at midlatitudes is lower than in the tropics and the view zenith angle is larger. As a result of this geometry, a dependence in ISCCP cloud fractions with latitude has long been recognized [*Rossow et al.*, 1993; *Evan et al.*, 2007]. At high latitudes (poleward of about 50°), ISCCP relies on polar orbiting satellite observations. The ISCCP data in Figure 11 (top left) certainly shows a large change in the amount of optically thick cloud near 50°S in the South Pacific that is not found in the MISR (top right) or MODIS (bottom right) data sets. Our case study scenes (which used ISCCP retrievals from geostationary satellites) for the South Pacific and North Pacific (not shown) also seem to have a similar shift in the distribution

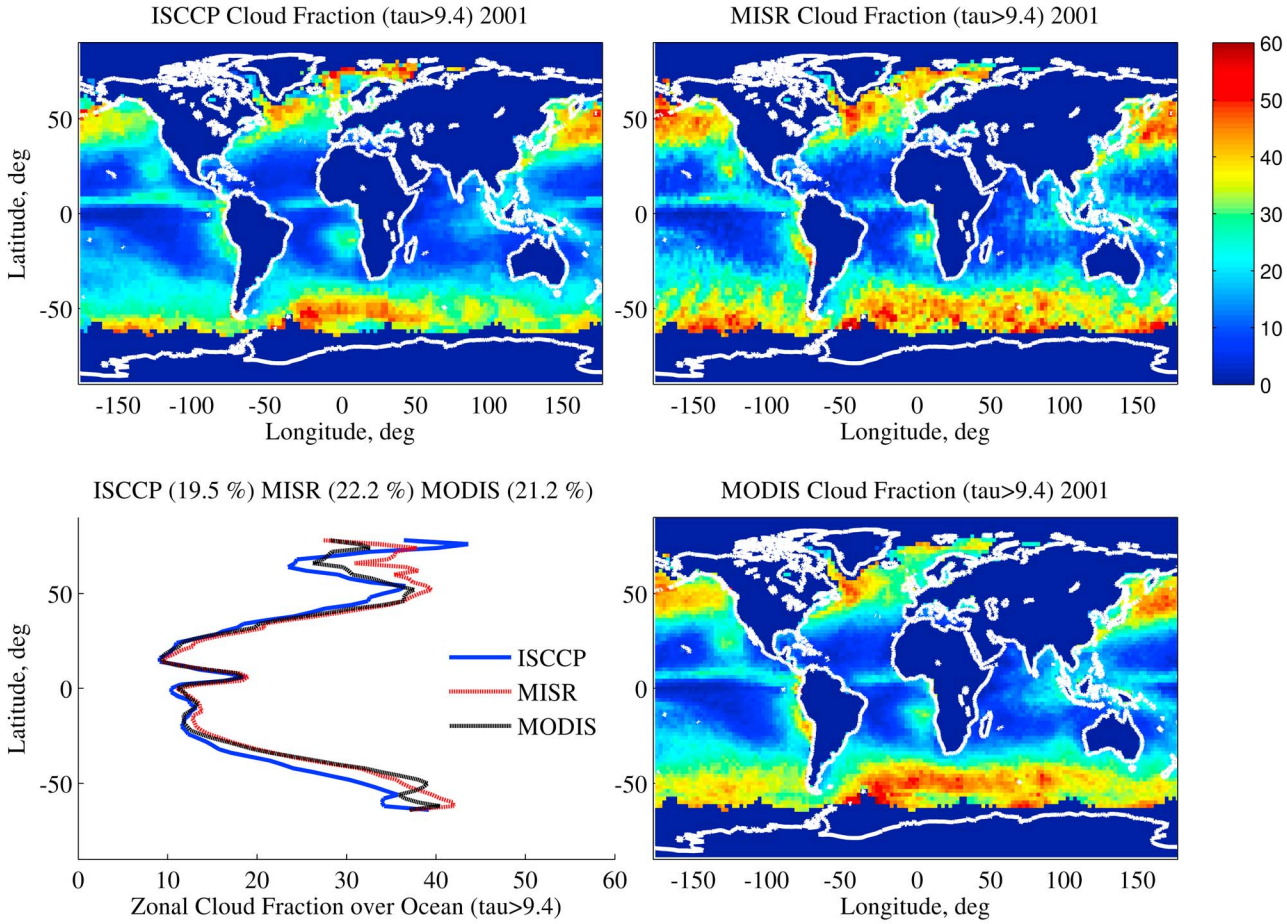

Figure 11. Total cloud cover (cloud tops at any altitude) but including only clouds with optical depths > 9.4. (Plots are as in Figure 9.)

of ISCCP cloud optical depth toward lower optical depths relative to that retrieved by MISR or MODIS. The shift seems to occur for both low-level and high-level clouds but was most distinct for multilayer clouds, which may at least partly explain why the differences with ISCCP shown in Figure 11 (bottom left) are larger in the Southern Hemisphere (which as we will see later in this section has more multilayer cloud). We speculate that this bias (difference) in optically thick cloud amount between ISCCP and MODIS/MISR at midlatitudes reflects a bias in optical depth retrievals based on one-dimensional radiative transfer with view and solar zenith angles. Nonetheless, other factors such as the cloud phase used in the retrieval and horizontal resolution may also be a factor and this topic needs to be studied further.

4.3. Midlevel and Multilayer Clouds

[37] Over most oceanic regions ISCCP identifies more midlevel cloud (440 hPA < cloud top pressure < 680 hPA) than either MISR or MODIS. The relatively large amounts of midlevel cloud identified by ISCCP are generally due to bias in the ISCCP retrieval of cloud top when multilayer clouds are present (see section 3.3, *Stubenrauch et al.* [1999], and *Rossow et al.* [2005]). As a result, we recommend that comparison of model output with ISCCP data should combine high-level and midlevel cloud amounts (rather than individually comparing model output to ISCCP high-level and midlevel fractions).

[38] Figure 12 compares the amount of ISCCP high-level + midlevel cloud with MISR high-level + midlevel cloud. As discussed earlier, the difference between these two quantities provides an estimate for the amount of multilayer cloud consisting of a low-level cloud and an optically thin upper-level cloud. Figure 12 shows that globally averaged such multilayer clouds occur about 13% of the time, with notably larger values throughout the tropical warm pool, in the North Pacific and North Atlantic, and at southern midlatitudes especially poleward of 50°. The large multilayer cloud fraction off the west coast of South America is an error in the estimate due to the aforementioned bias in ISCCP cloud tops in stratocumulus regions (see discussion in section 3.1). A variety of approaches for estimating the amount of multilayer cloud from satellite have been developed. *Heidinger and Pavolonis* [2005] developed a technique to identify multilayer cloud using NOAA's Advanced Very High Resolution Radiometer (AVHRR) data. The physical basis of their approach is to compare observations of the 0.63 μm reflectance with 10.8–12 μm brightness temperature difference. For single-layer clouds, plane parallel theory predicts a smooth relationship between these two quantities, which is violated when multiple cloud layers are present. The authors note that optimal performance of

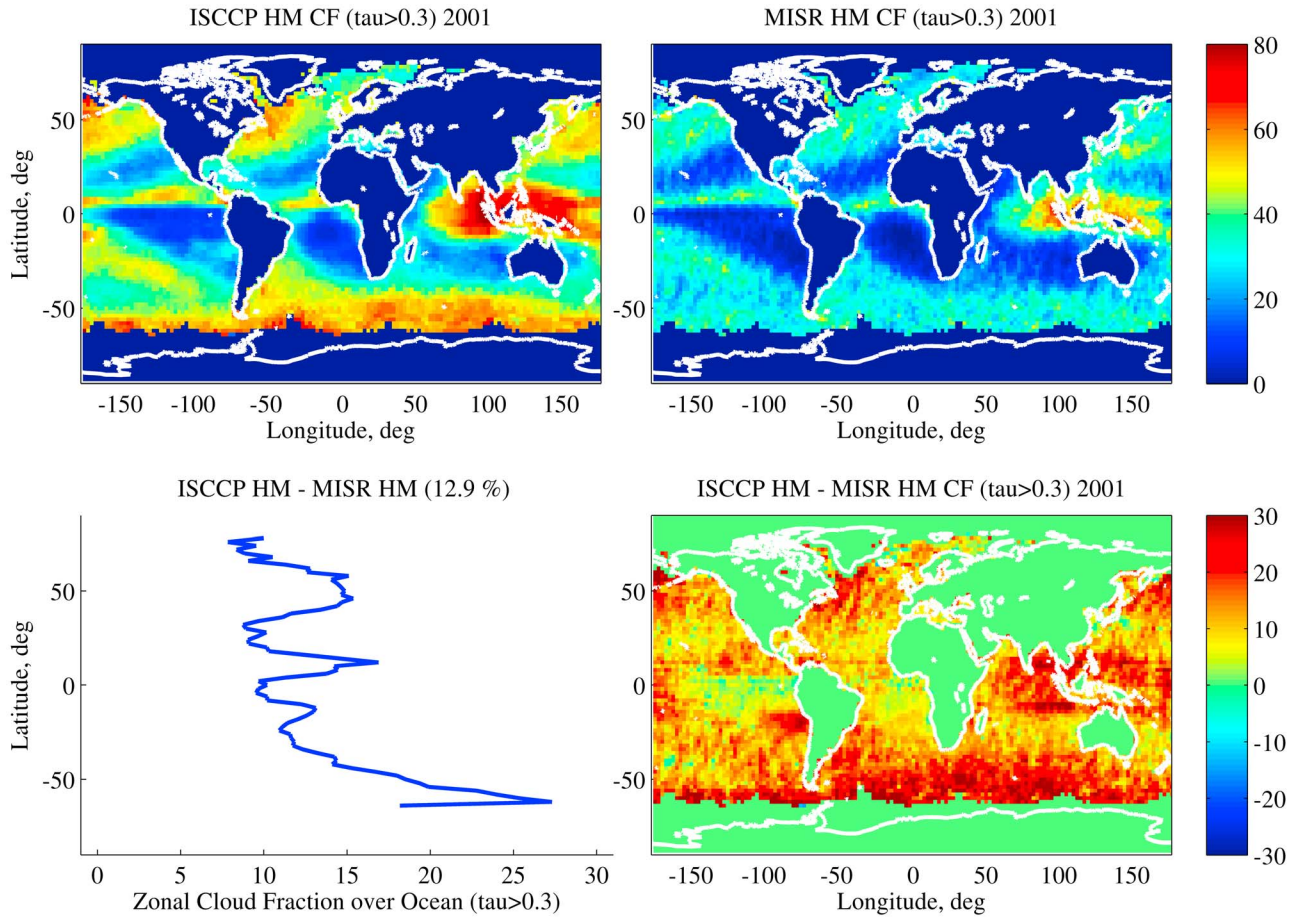

Figure 12. Estimate of multilayer cloud fraction from ISCCP and MISR. Includes only multilayer clouds where the upper-level cloud is optically thick enough for ISCCP to detect (optical depth > ~ 0.3) and optically thin enough that MISR can "see" through the cloud (optical depth < 1 to 2); see text. Estimate is given by ISCCP high-level + midlevel (HM) cloud amount minus the MISR high-level + midlevel (HM) cloud amount. (top left) ISCCP HM cloud fraction, (top right) MISR HM cloud fraction, (bottom right) multilayer cloud fraction (the difference between the top left and top right plots). (bottom left) Zonally averaged multilayer cloud fraction with the global (cosine weighted) average shown in panel title.

this method occurs when a cirrus cloud with an optical depth between 0.5 and 3 occurs over a lower and warmer cloud with an optical depth greater than 5. These are roughly the same conditions under which we have found that the MISR stereo retrieval will generally identify the altitude of the lower cloud. Heidinger and Pavolonis found the average multilayer cloud fraction between 60°N and 60°S to be 12% with regional values approaching 35% over the tropical warm pool and over the southern oceans, especially in July, similar to our result shown in Figure 12 (bottom). Also, similar to Heidinger and Pavolonis, we find that the global pattern of ISCCP and MISR multilayer cloud occurrence has a strong seasonal cycle, with the maximums tracking the annual shifts in position of the major tropical convective zones and midlatitude storm tracks (not shown). *Chang and Li* [2005] developed a method for identifying multilayer clouds using MODIS observations from the multispectral CO_2-slicing channels (13.3, 13.6, 13.9, and 14.2 m) and conventional VIS and IR window channels. They applied this technique to MODIS observations from January, April, July, and October 2001. They found a global multilayer cloud fraction over ocean of 12.3% and global patterns that are similar to those found by Heidinger and Pavolonis and to those shown in Figure 12. *Jin and Rossow* [1997] developed a technique to identify multilayer clouds using only brightness temperature differences in High-resolution Infrared Radiometer Sounder (HIRS) $C0_2$ channels at 13.3, 13.7, 14, and 14.2 μm. They found the frequency of occurrence of multilayer clouds over the ocean equatorward of 60° was 25.5% in July 1989 and 20.4% in January 1990. It is not immediately clear why this estimate is so much larger than that found by *Heidinger and Pavolonis* [2005], *Chang and Li* [2005] or here. (The article by Jin and Rossow is not very clear as to whether the multilayer fraction they estimate is the fraction relative to the total number of observations or to some other reference, for example, relative to the total amount of cloud or total amount of high cloud. If the later, this might partially explain this larger value. All the fractions stated here are relative to the total number of observations (in the given region) unless otherwise explicitly indicated.)

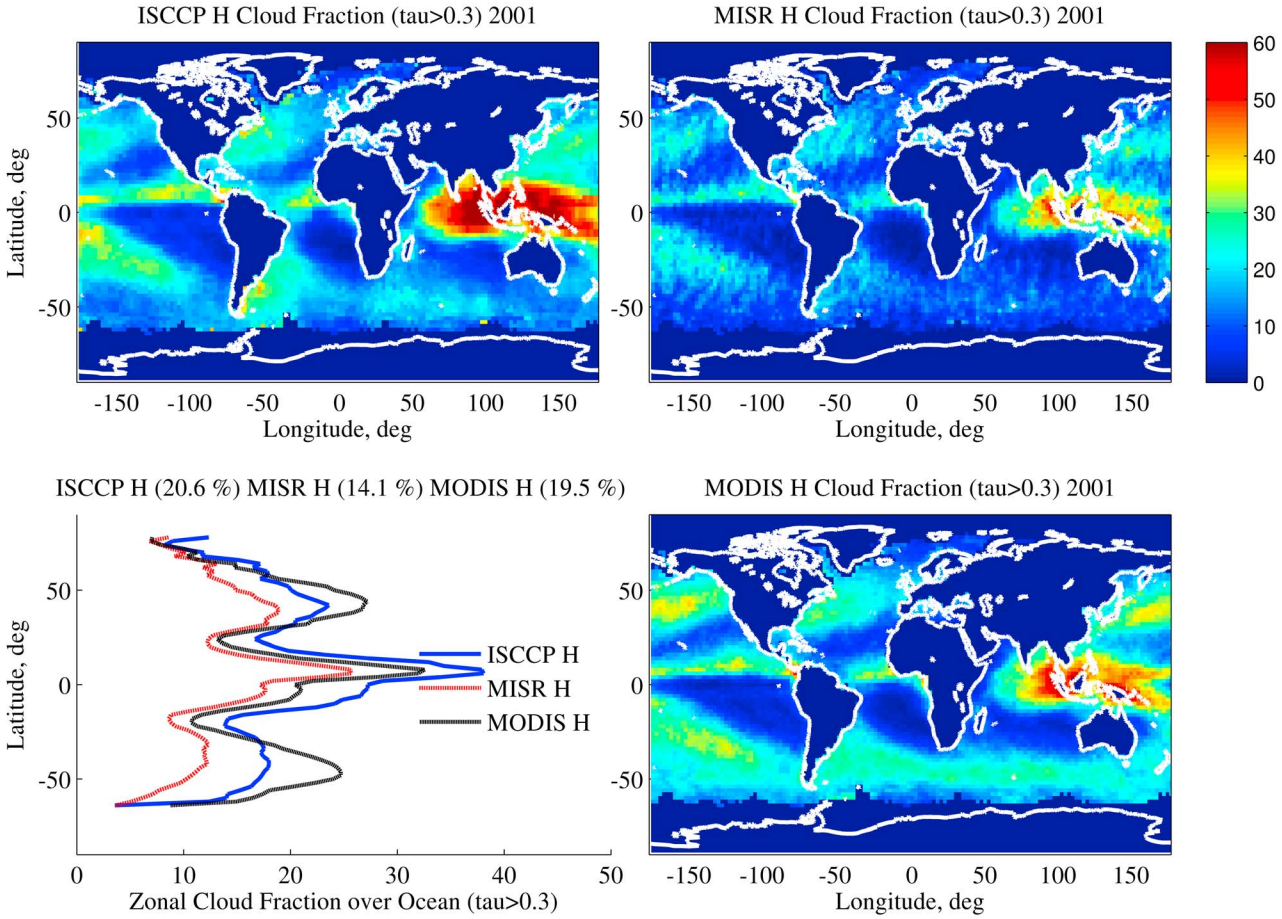

Figure 13. Comparison of high-level cloud amounts (cloud top pressure < 440 hPA), (top left) ISCCP, (top right) MISR, and (bottom right) MODIS. (bottom left) Comparison of zonal averages with the global (cosine weighted) average shown above the plot.

[39] Other efforts to determine multilayer cloud occurrence over ocean include research by *Minnis et al.* [2007], *Ho et al.* [2003] and *Lin et al.* [1998], who combine passive microwave data with passive infrared and visible imagery to estimate the occurrence of ice clouds over water clouds, *Mace et al.* [2009], who examined multilayer cloud occurrence in merged data from satellite cloud radar (CloudSat) and lidar (CALIPSO), and *Wang and Dessler* [2006], who examined cloud overlap in observations from the Geoscience Laser Altimeter System (GLAS) lidar carried aboard the Ice, Cloud, and Land Elevation Satellite (ICESat) in the tropics (between 10°S and 20°N). These data sets are difficult to compare directly with the results presented here because the passive microwave and radar data can penetrate most clouds (not just optically thin cirrus) and the lidar systems are likely more sensitive to the thin cirrus than passive instruments. Thus one expects these data may well have larger multilayer cloud occurrences. Wang and Dressler found tropical cirrus occurred 34.5% of the time over the tropical ocean with multilayer clouds occurring 18% of the time. Of this 18% about 4.5% was cirrus over other cirrus, which would not be identified in the ISCCP and MISR differences; the remaining 13.5% overlap is similar to the value found here for the same latitudes. Mace and coauthors find multilayer cloud layers 18% of time (with a global pattern that is similar to that shown in Figure 12 for thin cirrus), but they note this may well be an underestimate of the true overlap given the difficulties that CloudSat and CALIPSO have in detecting low-level clouds and differentiating them from aerosols. Multilayer cloud amounts derived by *Ho et al.* [2003] are closer to those found here than those presented by Mace, but the comparison is complicated because the passive microwave approach has coarse resolution (~20 km) and can only be applied over areas free of precipitation.

4.4. High-Level Clouds and the Tropical Western Pacific

[40] The global distribution of high-level clouds (cloud top pressure < 440 hPA) retrieved from ISCCP, MISR and MODIS is shown in Figure 13. Figure 13 (bottom left) compares zonal averages of the high cloud amount and indicates that at midlatitudes and high latitudes the MODIS joint histogram contains more high cloud, while in the tropics and subtropics ISCCP contains more high cloud. An examination of the ISCCP and MODIS joint histograms for the tropical western Pacific (10°N to 10°S, 130°E to 170°W), given in Figures 14a and 14b shows that the ISCCP high cloud fraction is larger than the MODIS fraction (in the

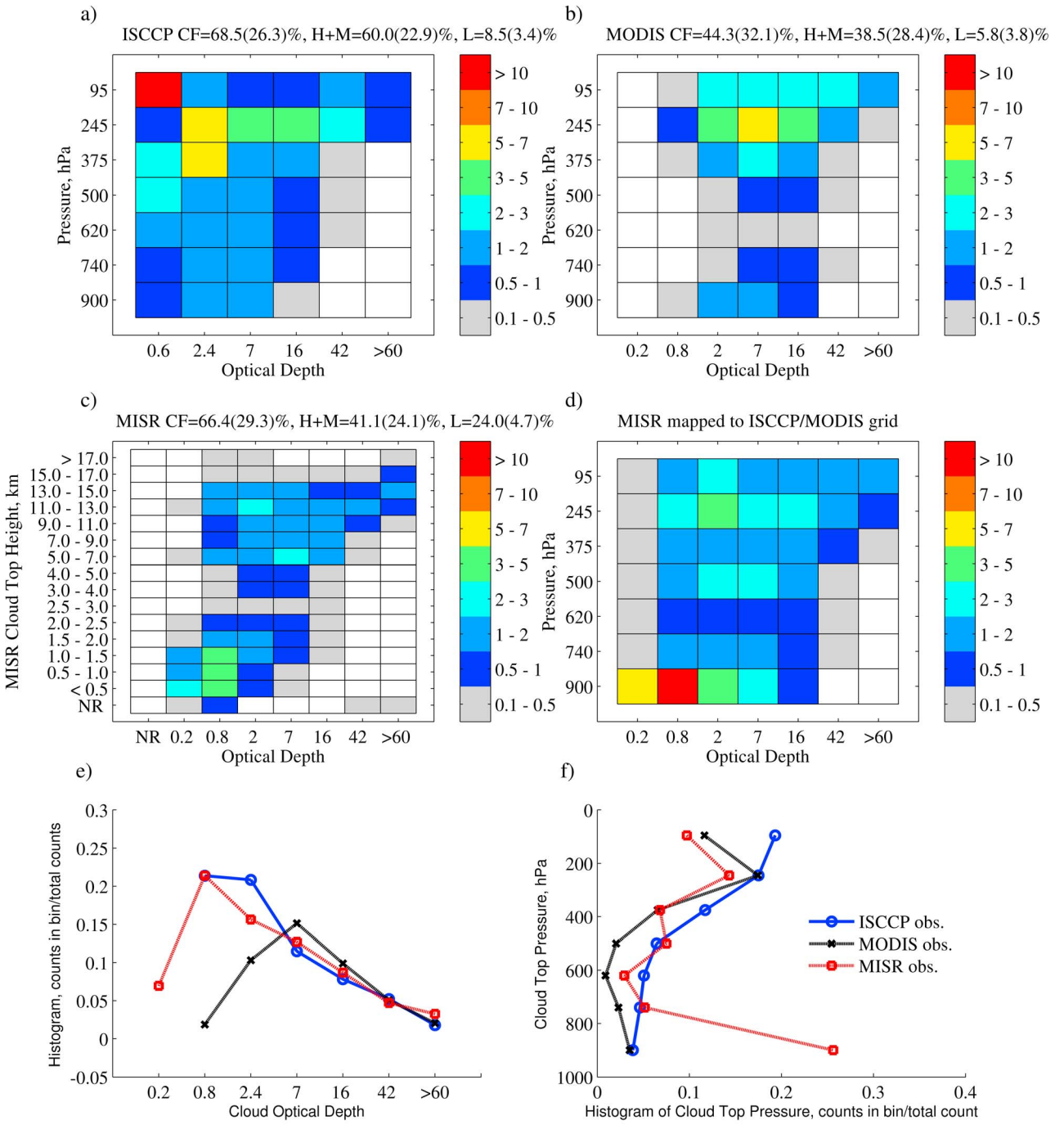

Figure 14. Same as Figure 7 but for the tropical western Pacific (10°N to 10°S, 130°E to 170°W).

tropics) because of the large amount of optically thin high-level cloud (optical depth less than 1.3) in the tropics. The MODIS optical depth retrieval is not applied to some of this thin cloud (see section 3.3). In addition, while cloud tops for some of this high-level cloud will be biased by ISCCP into midlevels, much of this cloud is single-layered and sufficiently optically thin that the ISCCP retrieval is assigning the altitude of this cloud to the lowest pressure and lowest optical depth bin (the upper left corner of the joint histogram in Figure 14a), as discussed in section 3.3. In contrast, in midlatitudes (e.g., in the North Pacific, Figures 7a and 7b) there is less optically thin high-level cloud, and a larger percentage of what exists is multilayered. The ISCCP high-level cloud tops are therefore more frequently biased into midlevels and little cloud is assigned to the lowest pressure bin.

[41] With regard to low clouds, the MISR histograms in Figures 14c and 14d show that almost all of the low cloud in this region (at least that which is visible from a spaceborne imager) has low (1D equivalent) optical depths, as expected

of small trade cumulus. This is true throughout most of the tropics and subtropics. These optical depths (derived based on one-dimensional radiative transfer) likely do not accurately reflect the true optical depth distribution, for which retrievals based on three-dimensional radiative transfer are needed.

[42] Another feature of particular interest in this region is the peak in cloud fraction observed by MISR between 5 and 7 km (Figure 14c). This altitude range typically includes the tropical freezing level, where a cloud layer has long been noted to preferentially form [*Johnson et al.*, 1999] and is frequently captured in cloud radar observations from the U.S. Department of Energy (DOE) Atmospheric Radiation Measurement (ARM) program tropical western Pacific sites [*Hollars et al.*, 2004; *McFarlane et al.*, 2007] and more recently by CloudSat [*Riley and Mapes*, 2008].

5. Summary and Discussion

[43] There are notable differences in the joint histograms of cloud top height and optical depth being produced by the ISCCP (D data sets), MODIS (MOD08, Collection 5) and MISR projects. These differences have their roots in the different algorithms used to detect clouds and to retrieve the cloud heights and optical depths. The differences in the three data sets are largely driven by responses of the retrievals to (1) low-level clouds under temperature inversions, (2) small (subpixel scale) and broken low-level clouds, and (3) multilayer clouds.

[44] Because each algorithm has different strengths and weakness, the combination of data sets tells us more about the observed cloud fields than any of the three by itself. In particular, the MISR stereo height retrieval provides a calibration insensitive approach to determining cloud height that is especially valuable in combination with ISCCP and MODIS data sets. This is because the combination provides a direct means to estimate the amount of multilayer cloud (with a low-level cloud below an optically thin midlevel or high-level cloud). The multilayer occurrence is found by subtracting the sum of high-level and midlevel cloud found by ISCCP (or MODIS) from the sum of high-level and midlevel cloud found by MISR. An estimate for the amount of single-layer low cloud amount in the MISR data set can likewise be made by subtracting the multilayer cloud amount from the total amount of MISR low cloud.

[45] We recommend, therefore, that evaluations of climate model output include comparison with both MISR and ISCCP joint histograms of cloud top height and optical depth. In addition to taking advantage of estimates in multilayer clouds and single-layer low clouds provided by the combination, the MISR data provide more accurate retrievals of cloud top height for low-level and midlevel clouds, more reliable discrimination of midlevel clouds from other clouds, and better detection of trade cumulus, while ISCCP provides greater sensitivity to thin cirrus than MISR, a much longer time series, and diurnal sampling (not available to either MISR or MODIS). Because ISCCP high-level cloud top heights are often biased low in altitude (often well into midlevels in multilayer conditions) or assigned to the lowest-pressure bin (when the total column optical depth is small), comparisons of model output with ISCCP observations of high-level and midlevel cloud should concentrate on the sum of high-level and midlevel cloud amounts. Optimally, such comparison should be undertaken using instrument simulators, as discussed in the companion paper to this article [*Marchand and Ackerman*, 2010].

[46] The above recommendations are not intended to imply that comparison with MISR and ISCCP should be undertaken exclusive of MODIS or other satellite data sets such as those being provided by CloudSat or CALIPSO. The analysis in section 4.1, for example, demonstrates the advantage of including the MODIS (MOD08) data set for analysis of optically thick clouds in combination with MISR and ISCCP.

[47] Since a primary purpose of the joint histograms produced by the ISCCP, MODIS and MISR projects is to provide observational data for the evaluation of climate models, it is important to understand the difference between the fraction of pixels containing a cloud (i.e., what the CTH-OD histograms contain) and the "true" fractional area covered by clouds (both of which are often referred to as cloud fraction). Because satellite pixels can be partially filled by clouds, the fraction of satellite pixels containing some amount of cloud (what one might call the "imager-retrieved" cloud fraction) will be larger than the true fractional area covered by clouds, and this difference should increase as the satellite pixel size is increased [*Di Girolamo and Davies*, 1997]. Of course, satellite retrievals do not perfectly identify partially cloud-filled pixels as cloudy. In fact, the comparisons presented in sections 3 and 4 show that MISR identifies a larger faction of pixels as cloudy than ISCCP (in regions dominated by small cumulus clouds) even though the pixel size (or effective resolution) of MISR (about 1.1 km) is smaller than ISCCP (4 km at nadir). Because of these failed detections, the imager-retrieved cloud fraction is closer to the true fractional area covered clouds than would be produced by a perfect cloud detector with the same resolution [*Wielicki and Parker*, 1992]. While in some sense beneficial for the evaluation of true cloud area (and perhaps sufficient for mean radiative fluxes) the difference between the "imager-retrieved" cloud fraction and the true cloud area will vary with location (depending on the size of cloud elements and other factors that influence the cloud detection), and the missing cloud detections may well distort the apparent distribution of retrieved cloud properties. The difference between the MISR and ISCCP imager-retrieved cloud fractions provides at least a rough estimate on the sensitivity of the retrieved cloud fractions to failed detections.

[48] In trade cumulus regions, the difference between the imager-retrieved cloud fraction and the true cloud area can be large. *Zhao and Di Girolamo* [2006] compared MISR and MODIS operational cloud masks (produced at 1.1 and 1 km, respectively) with cloud masks generated from 15 m resolution visible wavelength observations made by the Advanced Spaceborne Thermal Emission and Reflection (ASTER) imager (which also flies on board the NASA Terra space craft) for 124 scenes dominated by trade cumulus. They found the fraction of ASTER pixels identified as cloudy was about 8%. However, when the ASTER cloud mask was reduced in resolution to match the MISR and MODIS grids (with essentially perfect partially filled cloud detection), the fraction of pixels identified as cloud increased

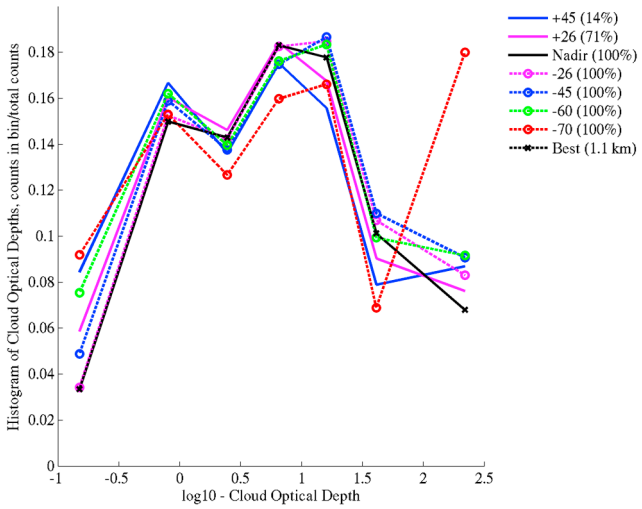

Figure A1. Distribution of MISR optical depths as a function of MISR camera/view angle in January 2001 for the North Pacific. The retrieval is only run for angles with little possibility of Sun glint. In each plot, the legend shows the percentage of the total possible observations (for each view angle) considered free of Sun glint. Also shown is the best camera result, which combines the results for camera closest to nadir which is considered free of Sun glint on a pixel-by-pixel basis. For the North Pacific, this is always the nadir camera but for the tropical western Pacific (Figure A2) this is a mix of the Nadir and 26° aft-view.

to about 50%. The MISR cloud mask algorithm correctly identified approximately 82% of the pixels that contained small (often subpixel) clouds with a total cloud fraction of 44%, while MODIS correctly identified 62% of the cloudy pixels with a total cloud fraction of 26%. It therefore appears that the MISR cloud mask is operating close to the nominal 1 km resolution cloud mask over deep ocean (meaning most partially filled pixels are detected as cloudy) and the MISR cloud fraction will be larger than the true fractional area covered by clouds.

[49] Based on the preceding discussion, we suggest that comparisons of the MISR joint histograms with model output be conducted in a manner consistent with nominal 1 km resolution cloud detection. From the climate model perspective, this may prove difficult because most climate models do not produce cloud fields in which the size and spacing of cloud elements is explicitly determined. An exception is the Multiscale Modeling Framework (MMF) approach in which most climate model cloud parameterizations are replaced with a two-dimensional or small three-dimensional cloud resolving model. In the companion paper to this article [*Marchand and Ackerman*, 2010], we examine the impact of resolution in comparing MMF model output with MISR and ISCCP joint histograms. As one would expect, the impact of the finite 1 km resolution is largest in regions dominated by trade cumulus. Alternatively, rather than trying to simulate 1 km resolution cloud masking from model output, it may prove better to design more sophisticated algorithms to estimate the true cloud area from the satellite observations (rather than treating the fraction of pixels with clouds as the true cloud fraction). Techniques to make such estimates have been proposed [e.g., *Di Girolamo and Davies*, 1997], but more research in this area (especially in regard to uncertainty) is needed. We hope that future NASA satellite missions will focus on continuous observations at spatial resolutions higher than that of either the MISR or MODIS missions, in order to improve cloud detection and to enable retrievals that consider both the three dimensional structure of clouds and the interaction of visible photons with clouds and aerosols in close proximity.

Appendix A: Additional Details on MISR CTH and OD Retrievals

[50] The MISR CTH-OD histograms use the MISR best-winds retrieval, when a high-quality wind retrieval is obtained and otherwise use the retrieved height without any wind correction (i.e., the MISR without-winds retrieval). The heights are also spatially filtered using a 12 × 12 km median following the analysis of *Marchand et al.* [2007], who showed that such filtering produced good agreement with cloud radar observations of CTH. The optical depth retrieval is only run for pixels determined to be cloudy (with high confidence) by the MISR radiometric cloud mask, described by *Zhao and Di Girolamo* [2004]. The radiometric cloud mask is based on thresholding of observed visible reflectances and the standard deviation of the 275 m reflectances at a scale of 1.1 km. The cloud mask has been found to compare well with a nominal cloud mask at 1.1 km resolution when tested using 15 m imagery collected by the ASTER instrument in trade cumulus dominated scenes [*Zhao and Di Girolamo*, 2006]. While the surface reflectance is small, it is nonetheless accounted for using an anisotropic ocean model following ISCCP. Clouds with a CTH below the climatological freezing level are assumed to be composed of water drops with an effective radius of 10 μm, while those above the freezing level are treated as ice particles with an effective radius 50 μm and an aggregate-like crystal habit. *McFarlane et al.* [2007] found that this aggregate model fits the angular scattering pattern observed by all nine MISR view angles well much of the time. The underlying scattering phase function used in the MISR retrieval is very similar to that used in ISCCP, which has likewise been found to match multiangle reflectance measurements reasonably well [*Doutriaux-Boucher et al.*, 2000; *Descloitres et al.*, 1998].

[51] While there has been some research into the potential advantage of using multiple MISR view angles for cloud optical depth retrieval [*Evans et al.*, 2008; *McFarlane and Marchand*, 2008] much more research is needed and no operational multiangle retrievals yet exist. Only one MISR camera (that is, one view angle) is used in the optical depth retrieval. However, the results shown here take advantage of the MISR multiangle cameras by selecting a best camera, as the camera closest to nadir that has no Sun glint. Most of the time, the best camera is either the nadir viewing camera, or one of the MISR 26° cameras. There is however, a small region in the tropics (the exact location of which moves with the seasonal cycle) where a 45° view is used. In general, three-dimensional scattering effects can cause individual

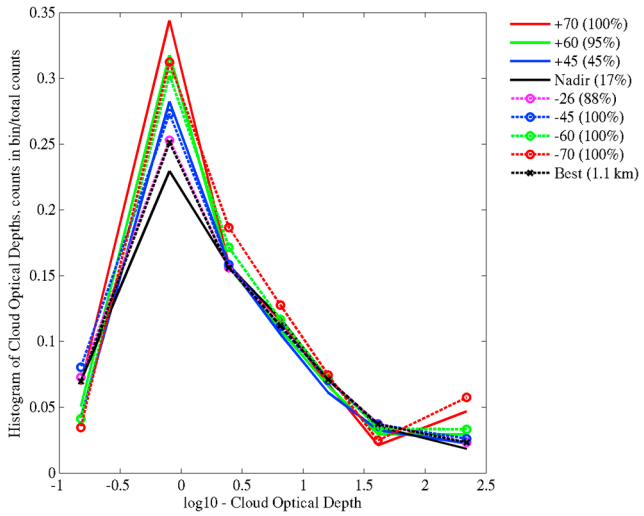

Figure A2. Same as Figure A1 but for the tropical western Pacific, July 2001.

cloudy pixels to appear brighter or darker than would be the case for a plane-parallel (or one-dimensional) cloud with the same optical properties. The MISR resolution (field of view) also changes with view angle. With the coarse optical depth bin size employed here, however, the difference between the retrieved optical depth histograms obtained from the various MISR cameras is generally small (except for the most oblique viewing cameras).

[52] The MISR joint histogram data set contains both the "best camera" result, as well as histograms for each of the 9 MISR views. This permits examination of the sensitivity of the MISR retrieval to the view angle. Figure A1, for example, shows results for the North Pacific, and Figure A2 shows results for the tropical western Pacific. Except for the most oblique MISR view angles (green and red lines), Figures A1 and A2 show that view angle has only a modest effect on the optical depth distribution. Note that the legend in each panel shows the percentage of the total possible observations (for each view angle) considered free of Sun glint. As expected, the total cloud fraction increases as the view zenith angle increases because one can increasingly view the "sides" of clouds and because longer slant paths make thin cirrus easier to detect. The view angle effect is often most pronounced in regions with broken clouds and thin cirrus, which dominate the distribution in the tropics. The effect of view angle on the retrieval also generally increases as the solar zenith angle increases. It is largest for the North Pacific in January and changes very little with the season in the tropics (not shown).

[53] The relatively modest sensitivity to view angle should not be taken to mean that the optical depth of individual pixels remains the same regardless of view angle. Rather, it shows that (given the size of the optical depth bins in the histogram) the net change in the optical depth distribution is not typically large. This result is consistent with previous studies, such as that by *Várnai and Marshak* [2007], who found that mean optical depth retrieved from MODIS shows little sensitivity to view angle for solar zenith angles less than about 50°, and *Horváth and Davies* [2004] who found that the percentage of clouds for which MISR observations fit plane-parallel model increases dramatically if the MISR 60° and 70.5° views are not considered.

Appendix B: Additional Details on MODIS CTH and OD Retrievals

[54] The MODIS optical depth retrieval (in MOD06) assumes single-layer single-phase clouds and a variety of tests (using observations from several MODIS solar reflectance and IR channels) are applied to determine the cloud phase. Ice cloud scattering is treated using a mixture of ice habits, and retrievals for both ice and liquid water clouds are based on one-dimensional radiative transfer [*Baum et al.*, 2005]. The latest version of MOD06 (Collection 5) also includes a multilayer flag using, in part, a near-infrared absorption technique. Theoretical studies of the multilayer detection algorithm have been described along with example results by *Wind et al.* [2010] and quantitative validation is ongoing and includes the CloudSat study by *Joiner et al.* [2010]. An additional 1.6–2.1 μm band combination is also calculated in MOD06 over snow/ice surfaces, but is not used in MOD08.

[55] All MOD08 statistics (scalars and histograms) are obtained by sampling the native 1 km optical depth retrieval in the MOD06 product for each 5 × 5 pixel group. There is only one cloud top pressure retrieval for each such group of 5 × 5 (1 km) pixels. *Oreopoulos* [2005] examined the impact of this sampling on the MODIS summaries. At the temporal and spatial scales used in section 4, the impact appears to be small.

[56] In MOD08, in addition to "clear-sky restoral" filter described in section 2, optical depths from those liquid water pixels which are found to have an effective radius of 30 μm (the maximum size range allowable by the retrieval) are not included. This is because an effective radius of 30 μm is often indicative of three-dimensional scattering effects, multilayer scenes (overlying ice phase contamination), an incorrectly retrieved cloud phase, a mixed phase cloud, a significant precipitation mode, or false cloud detection – and so a 30 μm retrieval value is interpreted as a failed retrieval. The effect of this filtering appears to be minor relative to the reduction in cloud coverage due to the clear-sky restoral. Because of the reduced coverage, users should also examine the MODIS total cloud fraction (MOD08 variable Cloud_Fraction_Day), which gives the cloud fraction for all clouds identified in the MOD35 cloud mask.

[57] Last, we while we only examined the MOD08 ISCCP-like histograms of cloud top pressure and optical depth in this article, the MOD08 product also contains optical depth histograms generated separately for the water and ice phases, joint histograms of optical depth versus effective radius, cloud top temperature, and effective emissivity, as well as effective radius binned against cloud top temperature and effective emissivity. Cloud properties for single-layer and multilayer clouds are aggregated separately using the MOD06 multilayer flag. As with the joint histograms of cloud top pressure and optical depth, these other statistics use only the standard optical depth and effective radius retrieval (using the 2.1 μm band) and are similarly filtered (e.g., "clear sky restoral" and ignoring the retrieval

when water cloud effective radii are less than or equal to 4 μm or equal to 30 μm). This choice reflects a belief that the quality of the optical depth is correlated with a successful size retrieval and ensures the meaning and consistency of all joint histograms (some of which include effective radius) in the MOD08 data.

[58] **Acknowledgments.** The authors would like to express thanks to all those members of the NASA ISCCP, MODIS, and MISR teams who helped make this research possible, especially Jeff Walters at the NASA Langley Research Center (LaRC), who devoted considerable effort to processing the MISR data. We especially thank Amy Braverman (NASA JPL), who repeatedly insisted that the MISR project undertake creation of the joint histogram data set and somehow cornered us (R.M. and T.P.A.) into it. Special thanks also go to Steven Platnick and Steve Ackerman (of the MODIS team) for reviewing this article and for the many long discussions and valuable insights. We also thank Dave Diner (NASA JPL) for his leadership of the MISR science team, and we thank the MISR project, whose financial support made this research possible. MISR data were obtained from the NASA Langley Research Center Atmospheric Science Data Center. This research was funded by the NASA Jet Propulsion Laboratory (contract NMO710860).

References

Ackerman, S. A., R. E. Holz, R. Frey, E. W. Eloranta, B. C. Maddux, and M. McGill (2008), Cloud detection with MODIS. Part II: Validation, *J. Atmos. Oceanic Technol.*, *25*, 1073–1086, doi:10.1175/2007JTECHA1053.1.

Baum, B. A., and B. A. Wielicki (1994), Cirrus cloud retrieval using infrared sounding data: Multilevel cloud errors, *J. Appl. Meteorol.*, *33*, 107–117, doi:10.1175/1520-0450(1994)033<0107:CCRUIS>2.0.CO;2.

Baum, B. A., P. Yang, A. J. Heymsfield, S. Platnick, M. D. King, Y. X. Hu, and S. M. Thomas (2005), Bulk scattering properties for the remote sensing of ice clouds. 2: Narrowband models, *J. Appl. Meteorol.*, *44*, 1896–1911, doi:10.1175/JAM2309.1.

Chang, F., and Z. Li (2005), A Near-global climatology of single layer and overlapped clouds and their optical properties retrieved from *Terra*/MODIS data using a new algorithm, *J. Clim.*, *18*, 4752–4771, doi:10.1175/JCLI3553.1.

Descloitres, J., J. C. Buriez, F. Parol, and Y. Fouquart (1998), POLDER observations of cloud bidirectional reflectances compared to a plane-parallel model using the International Satellite Cloud Climatology Project cloud phase functions, *J. Geophys. Res.*, *103*(D10), 11,411–11,418, doi:10.1029/98JD00592.

Dessler, A. E., and P. Yang (2003), The distribution of tropical thin cirrus clouds inferred from Terra MODIS data, *J. Clim.*, *16*, 1241–1247, doi:10.1175/1520-0442(2003)16<1241:TDOTTC>2.0.CO;2.

Di Girolamo, L., and R. Davies (1997), Cloud fraction errors caused by finite resolution measurements, *J. Geophys. Res.*, *102*(D2), 1739–1756, doi:10.1029/96JD02663.

Diner, D. J., J. C. Beckert, G. W. Bothwell, and J. I. Rodriguez (2002), Performance of the MISR instrument during its first 20 months in Earth orbit, *IEEE Trans. Geosci. Remote Sens.*, *40*, 1449–1466.

Diner, D., et al. (2005), The value of multiangle measurements for retrieving structurally and radiatively consistent properties of clouds, aerosols, and surfaces, *Remote Sens. Environ.*, *97*(4), 495–518, doi:10.1016/j.rse.2005.06.006.

Doutriaux-Boucher, M., J.-C. Buriez, G. Brogniez, L. C. Labonnote, and A. J. Baran (2000), Sensitivity of retrieved POLDER directional cloud optical thickness to various ice particle models, *Geophys. Res. Lett.*, *27*(1), 109–112, doi:10.1029/1999GL010870.

Evan, A. T., A. K. Heidinger, and D. J. Vimont (2007), Arguments against a physical long-term trend in global ISCCP cloud amounts, *Geophys. Res. Lett.*, *34*, L04701, doi:10.1029/2006GL028083.

Evans, K. F., A. Marshak, and T. Várnai (2008), The potential for improved boundary layer cloud optical depth retrievals from the multiple directions of MISR, *J. Atmos. Sci.*, *65*, 3179–3196, doi:10.1175/2008JAS2627.1.

Frey, R. A., B. A. Baum, W. P. Menzel, S. A. Ackerman, C. C. Moeller, and J. D. Spinhirne (1999), A comparison of cloud top heights computed from airborne lidar and MAS radiance data using CO_2 slicing, *J. Geophys. Res.*, *104*(D20), 24,547–24,555, doi:10.1029/1999JD900796.

Garay, M. J., S. P. de Szoeke, and C. M. Moroney (2008), Comparison of marine stratocumulus cloud top heights in the southeastern Pacific retrieved from satellites with coincident ship-based observations, *J. Geophys. Res.*, *113*, D18204, doi:10.1029/2008JD009975.

Harshvardhan, G. Zhao, L. Di Girolamo, and R. N. Green (2009), Satellite-observed location of stratocumulus cloud-top heights in the presence of strong inversions, *IEEE Trans. Geosci. Remote Sens.*, *47*, 1421–1428, doi:10.1109/TGRS.2008.2005406.

Heidinger, A. K., and M. J. Pavolonis (2005), Global daytime distribution of overlapping cirrus cloud from NOAA's Advanced Very High Resolution Radiometer, *J. Clim.*, *18*, 4772–4784, doi:10.1175/JCLI3535.1.

Hinkelman, L. M., R. T. Marchand, and T. P. Ackerman (2009), Evaluation of Multiangle Imaging Spectroradiometer cloud motion vectors using NOAA radar wind profiler data, *J. Geophys. Res.*, *114*, D21207, doi:10.1029/2008JD011107.

Ho, S.-P., B. Lin, P. Minnis, and T.-F. Fan (2003), Estimates of cloud vertical structure and water amount over tropical oceans using VIRS and TMI data, *J. Geophys. Res.*, *108*(D14), 4419, doi:10.1029/2002JD003298.

Hollars, S., Q. Fu, J. Comstock, and T. Ackerman (2004), Comparison of cloud-top height retrieval from ground-based 35 GHz MMCR and GMS-5 satellite observations at ARM TWP Manus site, *Atmos. Res.*, *72*, 169–186, doi:10.1016/j.atmosres.2004.03.015.

Holz, R. E., S. A. Ackerman, F. W. Nagle, R. Frey, S. Dutcher, R. E. Kuehn, M. A. Vaughan, and B. Baum (2008), Global Moderate Resolution Imaging Spectroradiometer (MODIS) cloud detection and height evaluation using CALIOP, *J. Geophys. Res.*, *113*, D00A19, doi:10.1029/2008JD009837.

Horváth, Á., and R. Davies (2004), Anisotropy of water cloud reflectance: A comparison of measurements and 1D theory, *Geophys. Res. Lett.*, *31*, L01102, doi:10.1029/2003GL018386.

Jin, Y., and W. B. Rossow (1997), Detection of cirrus overlapping low-level clouds, *J. Geophys. Res.*, *102*(D2), 1727–1737, doi:10.1029/96JD02996.

Johnson, R. H., T. M. Rickenbach, S. A. Rutledge, P. E. Ciesielski, and W. H. Schubert (1999), Trimodal characteristics of tropical convection, *J. Clim.*, *12*, 2397–2418, doi:10.1175/1520-0442(1999)012<2397:TCOTC>2.0.CO;2.

Joiner, J., A. Vasilkov, P. K. Bhartia, G. Wind, S. Platnick, and W. P. Menzel (2010), Detection of multilayer and vertically extended clouds using the A-Train sensors, *Atmos. Meas. Tech.*, *3*(1), 233–247.

King, M. D., W. P. Menzel, Y. J. Kaufman, D. Tanré, B. C. Gao, S. Platnick, S. A. Ackerman, L. A. Remer, R. Pincus, and P. A. Hubanks (2003), Cloud and aerosol properties, precipitable water, and profiles of temperature and humidity from MODIS, *IEEE Trans. Geosci. Remote Sens.*, *41*, 442–458, doi:10.1109/TGRS.2002.808226.

Liao, X., W. B. Rossow, and D. Rind (1995), Comparison between SAGE II and ISCCP high-level clouds: 2. Locating cloud tops, *J. Geophys. Res.*, *100*(D1), 1137–1147, doi:10.1029/94JD02430.

Lin, B., P. Minnis, B. Wielicki, D. R. Doelling, R. Palikonda, D. F. Young, and T. Uttal (1998), Estimation of water cloud properties from satellite microwave, infrared and visible measurements in oceanic environments: 2. Results, *J. Geophys. Res.*, *103*(D4), 3887–3905, doi:10.1029/97JD02817.

Lin, W. Y., and M. H. Zhang (2004), Evaluation of clouds and their radiative effects simulated by the NCAR Community Atmospheric Model against satellite observations, *J. Clim.*, *17*, 3302–3318, doi:10.1175/1520-0442(2004)017<3302:EOCATR>2.0.CO;2.

Mace, G. G., Q. Zhang, M. Vaughan, R. Marchand, G. Stephens, C. Trepte, and D. Winker (2009), A description of hydrometeor layer occurrence statistics derived from the first year of merged CloudSat and CALIPSO data, *J. Geophys. Res.*, *114*, D00A26, doi:10.1029/2007JD009755.

Marchand, R., and T. Ackerman (2010), An analysis of cloud cover in multiscale modeling framework global climate model simulations using 4 and 1 km horizontal grids, *J. Geophys. Res.*, doi:10.1029/2009JD013423, in press.

Marchand, R. T., T. P. Ackerman, M. D. King, C. Moroney, R. Davies, J. P. Muller, and H. Gerber (2001), Multiangle observations of Arctic clouds from FIRE ACE: June 3, 1998, case study, *J. Geophys. Res.*, *106*(D14), 15,201–15,214, doi:10.1029/2000JD900302.

Marchand, R. T., T. P. Ackerman, and C. Moroney (2007), An assessment of Multiangle Imaging Spectroradiometer (MISR) stereo-derived cloud top heights and cloud top winds using ground-based radar, lidar, and microwave radiometers, *J. Geophys. Res.*, *112*, D06204, doi:10.1029/2006JD007091.

McFarlane, S. A., and R. T. Marchand (2008), Analysis of ice crystal habits derived from MISR and MODIS observations over the ARM Southern Great Plains site, *J. Geophys. Res.*, *113*, D07209, doi:10.1029/2007JD009191.

McFarlane, S. A., J. H. Mather, and T. P. Ackerman (2007), Analysis of tropical radiative heating profiles: A comparison of models and observations, *J. Geophys. Res.*, *112*, D14218, doi:10.1029/2006JD008290.

Menzel, W. P., R. A. Frey, H. Zhang, D. P. Wylie, C. C. Moeller, R. E. Holz, B. Maddux, B. A. Baum, K. I. Strabala, and L. E. Gumley (2008), MODIS global cloud-top pressure and amount estimation: Algorithm description and results, *J. Appl. Meteorol. Climatol.*, *47*, 1175–1198, doi:10.1175/2007JAMC1705.1.

Minnis, P., D. F. Young, C. W. Fairall, and J. B. Snider (1992), Stratocumulus cloud properties form simultaneous satellite and island-based instrumentation during FIRE, *J. Appl. Meteorol.*, *31*, 317–339, doi:10.1175/1520-0450(1992)031<0317:SCPDFS>2.0.CO;2.

Minnis, P., J. Huang, B. Lin, Y. Yi, R. F. Arduini, T.-F. Fan, J. K. Ayers, and G. G. Mace (2007), Ice cloud properties in ice-over-water cloud systems using Tropical Rainfall Measuring Mission (TRMM) visible and infrared scanner and TRMM Microwave Imager data, *J. Geophys. Res.*, *112*, D06206, doi:10.1029/2006JD007626.

Moroney, C., R. Davies, and J.-P. Muller (2002), Operational retrieval of cloud-top heights using MISR data, *IEEE Trans. Geosci. Remote Sens.*, *40*, 1532–1540, doi:10.1109/TGRS.2002.801150.

Muller, J.-P., A. Mandanayake, C. Moroney, R. Davies, D. J. Diner, and S. Paradise (2002), MISR stereoscopic image matchers: Techniques and results, *IEEE Trans. Geosci. Remote Sens.*, *40*, 1547–1559, doi:10.1109/TGRS.2002.801160.

Naud, C., J.-P. Muller, and E.E. Clothiaux (2002), Comparison of cloud top heights derived from MISR stereo and MODIS CO_2-slicing, *Geophys. Res. Lett.*, *29*(10), 1795, doi:10.1029/2002GL015460.

Naud, C., J.-P. Muller, M. Haeffelin, Y. Morille, and A. Delaval (2004), Assessment of MISR and MODIS cloud top heights through intercomparison with a back-scattering lidar at SIRTA, *Geophys. Res. Lett.*, *31*, L04114, doi:10.1029/2003GL018976.

Naud, C. M., J.-P. Muller, E. E. Clothiaux, B. A. Baum, and W. P. Menzel (2005), Intercomparison of multiple years of MODIS, MISR and radar cloud-top heights, *Ann. Geophys.*, *23*, 1–10.

Norris, J. R., and C. P. Weaver (2001), Improved techniques for evaluating GCM cloudiness applied to the NCAR CCM3, *J. Clim.*, *14*, 2540–2550, doi:10.1175/1520-0442(2001)014<2540:ITFEGC>2.0.CO;2.

Oreopoulos, L. (2005), The impact of subsampling on MODIS level-3 statistics of cloud optical thickness and effective radius, *IEEE Trans. Geosci. Remote Sens.*, *43*, 366–373, doi:10.1109/TGRS.2004.841247.

Platnick, S., M. D. King, S. A. Ackerman, W. P. Menzel, B. A. Baum, J. C. Riédi, and R. A. Frey (2003), The MODIS cloud products: Algorithms and examples from Terra, *IEEE Trans. Geosci. Remote Sens.*, *41*, 459–473, doi:10.1109/TGRS.2002.808301.

Riley, E. M., and B. E. Mapes (2008), Bimodal peak in mid-level tropical layer clouds observed by CloudSat, paper presented at 28th Conference on Hurricanes and Tropical Meteorology, Am. Meteorol. Soc., Orlando, Fla. (Available at http://ams.confex.com/ams/28Hurricanes/techprogram/MEETING.HTM)

Rossow, W. B., and R. A. Schiffer (1999), Advances in understanding clouds from ISCCP, *Bull. Am. Meteorol. Soc.*, *80*, 2261–2287, doi:10.1175/1520-0477(1999)080<2261:AIUCFI>2.0.CO;2.

Rossow, W. B., A. W. Walker, and L. C. Garder (1993), Comparison of ISCCP and other cloud amounts, *J. Clim.*, *6*, 2394–2418, doi:10.1175/1520-0442(1993)006<2394:COIAOC>2.0.CO;2.

Rossow, W. B., Y. Zhang, and J. Wang (2005), A statistical model of cloud vertical structure based on reconciling cloud layer amounts inferred from satellites and radiosonde humidity profiles, *J. Clim.*, *18*, 3587–3605, doi:10.1175/JCLI3479.1.

Seiz, G., R. Davies, and A. Gruen (2006), Stereo cloud-top height retrieval with ASTER and MISR, *Int. J. Remote Sens.*, *27*, 1839–1853, doi:10.1080/01431160500380703.

Stubenrauch, C. J., W. B. Rossow, F. Cheruy, A. Chedin, and N. A. Scott (1999), Clouds as seen by satellite sounders (3I) and imagers (ISCCP). Part I: Evaluation of cloud parameters, *J. Clim.*, *12*, 2189–2213, doi:10.1175/1520-0442(1999)012<2189:CASBSS>2.0.CO;2.

Várnai, T., and A. Marshak (2007), View angle dependence of cloud optical thicknesses retrieved by Moderate Resolution Imaging Spectroradiometer (MODIS), *J. Geophys. Res.*, *112*, D06203, doi:10.1029/2005JD006912.

Wang, J., W. B. Rossow, T. Uttal, and M. Rozendaal (1999), Variability of cloud vertical structure during ASTEX observed from a combination of rawinsonde, radar, ceilometer, and satellite, *Mon. Weather Rev.*, *127*, 2484–2502, doi:10.1175/1520-0493(1999)127<2484:VOCVSD>2.0.CO;2.

Wang, L., and A. E. Dessler (2006), Instantaneous cloud overlap statistics in the tropical area revealed by ICESat/GLAS data, *Geophys. Res. Lett.*, *33*, L15804, doi:10.1029/2005GL024350.

Webb, M., C. Senior, S. Bony, and J. J. Morcrette (2001), Combining ERBE and ISCCP data to assess clouds in the Hadley Centre, ECMWF and LMD atmospheric climate models, *Clim. Dyn.*, *17*(12), 905–922, doi:10.1007/s003820100157.

Whiteman, D. N., et al. (2001), Raman lidar measurements of water vapor and cirrus clouds during the passage of Hurricane Bonnie, *J. Geophys. Res.*, *106*(D6), 5211–5225, doi:10.1029/2000JD900621.

Wielicki, B. A., and J. A. Coakley Jr. (1981), Cloud retrieval using infrared sounder data: Error analysis, *J. Appl. Meteorol.*, *20*, 157–169, doi:10.1175/1520-0450(1981)020<0157:CRUISD>2.0.CO;2.

Wielicki, B. A., and L. Parker (1992), On the determination of cloud cover from satellite sensors: The effect of sensor spatial resolution, *J. Geophys. Res.*, *97*(D12), 12,799–12,823, doi:10.1029/92JD01061.

Wind, G., S. Platnick, M. D. King, P. A. Hubanks, M. J. Pavolonis, A. K. Heidinger, B. A. Baum, and P. Yang (2010), Multilayer cloud detection with the MODIS near-infrared water vapor absorption band, *J. Appl. Meteorol. Climatol.*, in press.

Wyant, M. C., C. S. Bretherton, J. T. Bacmeister, J. T. Kiehl, I. M. Held, M. Zhao, S. A. Klein, and B. J. Soden (2006), A comparison of low-latitude cloud properties and their response to climate change in three AGCMs sorted into regimes using mid-tropospheric vertical velocity, *Clim. Dyn.*, *27*(2–3), 261–279.

Zhang, M. H., et al. (2005), Comparing clouds and their seasonal variations in 10 atmospheric general circulation models with satellite measurements, *J. Geophys. Res.*, *110*, D15S02, doi:10.1029/2004JD005021.

Zhao, G., and L. Di Girolamo (2004), A cloud fraction versus view angle technique for automatic in-scene evaluation of the MISR cloud mask, *J. Appl. Meteorol.*, *43*, 860–869, doi:10.1175/1520-0450(2004)043<0860:ACFVVA>2.0.CO;2.

Zhao, G., and L. Di Girolamo (2006), Cloud fraction errors for trade wind cumuli from EOS-Terra instruments, *Geophys. Res. Lett.*, *33*, L20802, doi:10.1029/2006GL027088.

Zhao, G., and L. Di Girolamo (2007), Statistics on the macrophysical properties of trade wind cumuli over the tropical western Atlantic, *J. Geophys. Res.*, *112*, D10204, doi:10.1029/2006JD007371.

T. Ackerman and R. Marchand, Joint Institute for the Study of the Atmosphere and Ocean, University of Washington, Box 355672, 3737 Brooklyn Ave. NE, Seattle, WA 98105, USA. (rojmarch@u.washington.edu)

W. B. Rossow, NOAA Cooperative Remote Sensing Science and Technology Center, City College of New York, 160 Convent Ave., New York, NY 10031, USA.

M. Smyth, Jet Propulsion Laboratory, 4800 Oak Grove Dr., Pasadena, CA 91109, USA.